ACS OMEGA

Open Access

This article is licensed under CC-BY-NC-ND 4.0

http://pubs.acs.org/journal/acsodf

Article

Chemical and Geological Properties of Shale Gas: In Situ Desorption of Lower Cambrian Niutitang Shale in the Micangshan Tectonic Zone of South Shaanxi, China

Xiaotao Zhang, Bin Shen,* Tao Tian,* Shizhen Li, Xuemin Xu, Jiajia Yang, Weilin Sun, and Jing Qin

Cite This: *ACS Omega* 2024, 9, 13764−13781

Read Online

ACCESS | Metrics & More | Article Recommendations

ABSTRACT: Shale gas was recently found in the Lower Cambrian Niutitang Formation (LCNF) of the Micangshan tectonic zone of south Shaanxi (MTZSS), but not in commercial quantities. To determine the laws governing the generation, enrichment, and desorption of shale gases in overmatured shale strata in the LCNF of MTZSS, we carried out in situ desorption experiments on nine shale core samples and got 168 desorbed gas samples at different phases of desorption. Also measured were the chemical and carbon isotopic compositions of these desorbed gas samples and the geochemical parameters of the shale core samples. CH_4 was the predominant hydrocarbon shale gas identified in the 82.06−98.48% range, suggesting that the gases were mainly dry. The nonhydrocarbon gases found were CO_2 and H_2. The CH_4 content of the desorbed gas samples dropped continuously during desorption, lowering the dryness index to 98.48 and 92.26% of the first and last desorbed shale gas, respectively. The change in the gas ratio during shale gas desorption proved that the adsorbability of the LCNF to the various gases follows the trend $H_2 > CO_2 > C_2H_6 > CH_4 > He$. Further, $\delta^{13}C_2H_6$ and $\delta^{13}CH_4$ become heavier during desorption, showing isotopic fractionation arising from the desorption-diffusion coeffect. As the desorption temperature increases, the value of $\delta^{13}CH_4$ increases because $^{12}CH_4$ is more sensitive to temperature than $^{13}CH_4$, so it is with the ethane. Similar to the LCNF shale gas in other areas of China, the desorbed shale gases are characteristic of carbon isotope reversal (CIR) ($\delta^{13}CH_4 > \delta^{13}C_2H_6$). The cracking of the residual soluble organic matter at the high overmaturity stage mixed with the cracking of kerogen at the early stage of maturation, causing CIR. Furthermore, the desorbed gas content was proportionally and inversely related to the CIR degree and final dryness index of the desorbed gas, respectively. Moreover, the carbon isotope fractionation degree of CH_4 and $\delta^{13}C_1$ of the last desorbed gas correlated positively with the desorbed gas content and the desorbed time of the gas. In conclusion, the four parameters are effective parameters for identifying shale gas sweet spots.

1. INTRODUCTION

Shale gas is a natural gas preserved at its site of origin.[1] It has become an essential part of China's energy resource since the commercial exploitation of shale gas at the Upper Odovician Wufeng and Lower Silurian Longmaxi Formations was successfully implemented in the Sichuan Basin.[2−4] Examples of such gas fields are Fuling (the largest shale gas field in China) and Weiyuan-Changning shale gas fields. The Lower Cambrian Niutitang Formation (LCNF), also called the Qiongzhusi Formation or Shuijingtuo Formation, is currently the shale gas of interest in potential strata in China, aside from the Upper Ordovician Wufeng and Lower Silurian Longmaxi Formations. There were significant LCNF shale gas exploration breakthroughs in the Sichuan Basin and its periphery in the past years.[3−10] However, the shale gas production of the Wufeng and Silurian Longmaxi Formation is much higher than that of the LCNF, having negligible commercial development.[11] In recent years, the LCNF shale gas exploration in MTZSS suggests that the LCNF is ideal for exploration.[10,12−14]

Shale gas is composed of free, adsorbed, and dissolved gases.[7,15] Several researchers have reported that shale gas exists predominantly in adsorbed and free states, with minimal dissolved forms.[16] Generally, adsorbed gas accounts for 20−85% of total shale gas content.[17] Consequently, it is vital to understand the adsorption−desorption phenomenon of shale gas toward production and commercialization.[18] In situ desorption of core samples in well sites using a shale gas

Received: October 23, 2023
Revised: February 18, 2024
Accepted: February 27, 2024
Published: March 12, 2024

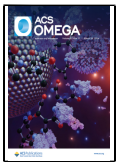

© 2024 The Authors. Published by American Chemical Society

https://doi.org/10.1021/acsomega.3c08330
ACS Omega 2024, 9, 13764−13781

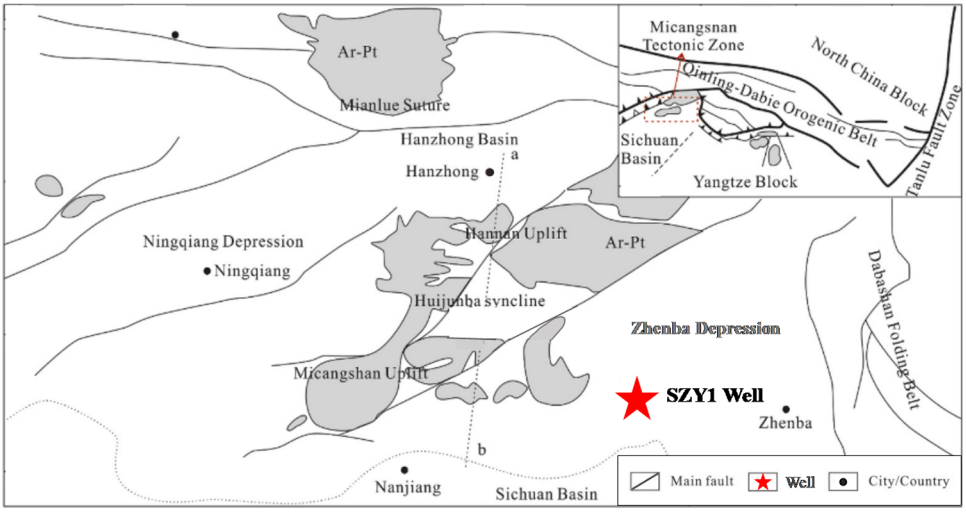

Figure 1. Locations of the Micangshan tectoni zone and the SZY1 well.

desorption apparatus is often adopted to study shale gas desorption behavior.[5,8,19,20] Afterward, chemical and isotopic changes of the constituent gases inform on the shale gas-bearing properties,[21] the proportion of free and adsorbed gas,[6,22] production,[9,23] and the genetic sources.[9,19,20]

Shale gas predominantly consists of methane (>94%), with fewer amounts of relatively high molecular weight hydrocarbon gases, such as (CH_4, C_2H_6, and C_3H_6), and minimum quantities of nonhydrocarbon gases, e.g., CO_2 and N_2.[24] However, many scholars have reported different gas components during production and desorption caused by the various adsorbability of the constituents.[5,9,20,25] Because different gas components with different molecular sizes show varying adsorption affinities in the microporous shales,[25] the ratios of different gas components indicate different variation trends with increasing desorbed time and temperature, for example, C_2H_6/CH_4 and have a generally rising trend with increasing desorbed time and temperature, whereas the CO2/C_2H_6 ratio has a decreasing trend with increasing desorbed time and temperature, elucidating that the order of the shale's absorption capacity for CH_4, C_2H_6, and CO_2, is determined as $CO_2 > C_2H_6 > CH_4$.[5,9,20,25]

The carbon isotopic values of the constituent gases are closely correlated with the evolutional thermal degree of the source rocks. The values are commonly utilized to distinguish coal-derived gas from shale-derived gas and thermogenic gas from biogenic gas.[19,26−30] More so, the carbon isotope fractionation has a profound impact on the carbon isotopic values.[5,8,20,25,31−34] The major factors affecting carbon isotope fractionation include the gas molecular weight,[35,36] physical properties of shales,[8,32,37] gas ratio,[33] and adsorption−desorption properties.[20,34,38]

Several shale gas exploration and production events have discovered CIR widely,[8,9,19,20,39−42] even in a shale gas reservoir in North America.[39,41] It was concluded that carbon isotope influences high shale gas production.[9] Although the genesis of CIR is controversial, it can be classified into four categories: (a) the secondary cracking of oils accompanied by kerogen cracking;[9,20,40,42,43] (b) the reaction between the shale kerogen and inorganics;[39,44] (c) the molecular diffusion of shale gas;[36,45] and (d) the adsorption−desorption behavior of shale gas.[20] The mixed gases derived from both the cracking of oils and kerogen are the most accepted opinion in interpreting the CIR. Moreover, gas wetness,[39,40] the role of water in hydrocarbon cracking,[39,44] and high maturity shale in a closed system[39,42,46] are the other factors influencing CIR. These factors are linked to the secondary cracking of oils accompanied by kerogen cracking. Therefore, the CIR is influenced by multiple parameters.

Presently, studies on shale gas of LCNF in MTZSS focus mainly on the relationship between Paleo-oxygen facies and organic matter enrichment,[14,47,48] hydrocarbon generation and accumulation of shale gas,[13] organic geochemical characteristics and the concomitant evaluation of shale source rocks,[10,49,50] reservoir characteristics of shale gas,[49,51,52] gas-bearing properties (total shale gas content),[49] and tectonic movement.[53,54] So far, no studies have been carried out on the compositional and isotopic characteristics of shale gas of LCNF in the MTZSS.

In the current study, desorbed gas samples were obtained using in situ desorption in the drilling site for shale gas exploration of the LCNF in MTZSS. Then, the gas samples were tested for chemical and carbon isotopic compositional changes during desorption. We explored the laws governing the generation, enrichment, and desorption of shale gases in overmatured shale strata, Also, we determined the order of the LCNF shale's absorption capacity for different gas components in MTZSS and proposed the CIR degree and final dryness index of the desorbed gas, the $\delta^{13}C_1$ and gas dryness index of the last desorbed gas samples can be effective indicators for identifying shale gas sweet spots. Our findings provide significant geological indications for further exploration and development of the LCNF shale gas in MTZSS.

2. SAMPLING AND EXPERIMENTS

2.1. Sampling. For this study, nine shale core samples of the SZY1 Well were collected, and 168 desorbed gas samples of the corresponding shale core samples were obtained through in situ desorption experiments during shale gas exploration of LCNF in the MTZSS. The Micangshan tectonic zone, consisting of five Secondary tectonic units, lies in the northern part of the Yangtze Platform. It is regarded as a transitional belt between the Sichuan Basin and Qinling Orogenic Belts[54] (Figure 1). By studying the Early Cambrian small skeletal fossils, previous studies have reported that the early Cambrian of the Micangshan tectonic zone is an independent terrane

https://doi.org/10.1021/acsomega.3c08330
ACS Omega 2024, 9, 13764−13781

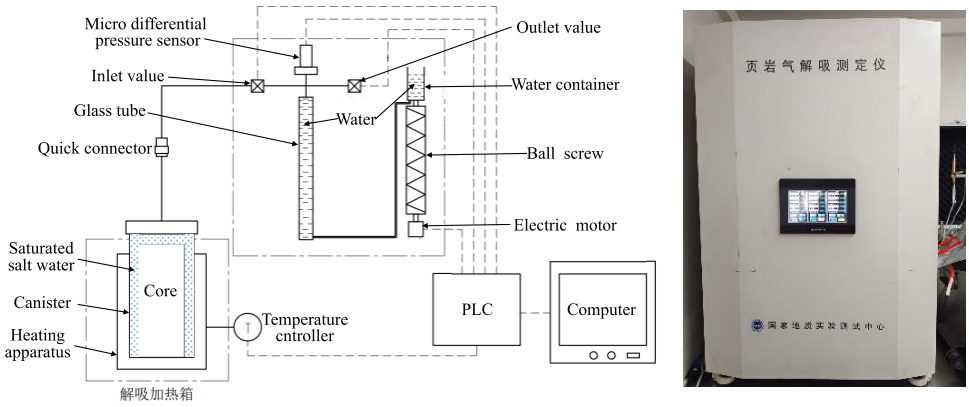

Figure 2. Schematic diagram of the instrument for shale gas desorption and in situ shale gas desorption experiments in the MTZSS (PLC = programmable logic controller).

rather than a part of the Upper Yangtze region.[22] The Niutitang Formation deposited black carbonaceous shale, with small amounts of gray-black shale and gray-black calcareous shale at the top and bottom, respectively. The LCNF shales of SZY1 Well, located in the east margin of Micangshan Uplift in MTZSS (Figure 1).

2.2. In Situ Shale Gas Desorption. A Petroleum and Natural Gas Industry Standard of the People's Republic of China "SY/T 6940−2020 Measurement method of shale gas content" was adopted for carrying out the in situ shale gas desorption measurements and calculating the gas content of shale samples. The in situ shale gas desorption experiments were carried out immediately after the shale core samples exited the core barrel and were sealed in the desorption canisters. The instrument for in situ shale gas desorption consists of heating, automatic metering, and data collection and processing parts (Figure 2). The whole workflow and working principle for measuring desorbed gas content are as follows: the core sampled from the wellbore of the drilling site was quickly put into a canister filled with saturated saltwater. The canister was covered tightly and sealed. The sealing time was recorded. After that, the pipe of the automatic meter was quickly plugged into the connector of the desorption canister. Meanwhile, the temperature controller was set in place.

The desorbed gas from the canister entered the glass tube filled with water through the inlet valve, resulting in a pressure difference between the water tube and the water container. The information was fed to the Programmable logic controller (PLC), which rapidly transmitted the processed signal to the servo motor. The motor then drove the ball screw to rotate, pushing the water container down and keeping the liquid level of the glass tube and the water container consistent. When the water container drops about 2/3 of the glass tube length, the inlet valve is closed. In contrast, the outlet valve is opened to discharge the desorbed gas collected in the gas bag if necessary. The liquid level of the glass tube and the water container rose and returned to the zero interface. Then, the desorbed gas was quantitated according to the PLC data using eq 1:

$$V_d = \pi\left(\frac{d}{2}\right)2 \times D$$

where, V_d is the volume of desorbed gases, d is the diameter of the glass tube, and D is the descending distance of the water container. All real-time data from PLC were transmitted to the computer, and specialized software recorded, further processed, and visualized the data. Also, variation trends, such as the trend of desorbed gas content and desorption temperature with desorbed time, were observed.

According to the heating procedure, the shale gas desorption experiment was divided into three phases: In Phase I, the desorption temperature was maintained at mud temperature (30 °C) for 3 h; in Phase II, the desorption temperature was raised to strata temperature (60 °C) over 1 h and maintained for 10 h; In Phase III, the desorption temperature was further elevated to 80 °C over 1 h and then held until the desorption ended. At 80 °C, prompt shale gas desorption was ensured without delaying the drilling. Moreover, the lasting desorbed time differs among the shale core samples because of the differences in the drilling time.

2.3. Laboratory Experiments. Laboratory experiments were performed at the National Research Center for Geoanalysis (NRCGA) in Beijing, China. Rock-eval pyrolysis and TOC measurements were conducted using a Rock-Eval 6 instrument and LECO CS-230H carbon/sulfur analyzer, respectively.[55] The shale samples were crushed to 1−2 mm particles, then coldly embedded with epoxy resin, and the surface of the thin section needed to be polished to no mechanical scratches by using an automatic polishing machine. After that, a Zeiss Axioimager II microscope system equipped with an ultraviolet light source and Diskus-Fossil system carried out the R_b measurements and maceral observation,[56−58] and two Petroleum and Natural Gas Industry Standards of the People's Republic of China-"SY/T 5124-2012 Method of determining microscopically the reflectance of vitrinite in sedimentary" and "SY/T 6414-2014 Maceral identification and statistical methods on polished surfaces of whole rocks" were adopted to determine the R_b and maceral observation of shale samples. Based on these two standards, the number of particles counted for R_b and maceral observation should not be less than 30 points and 800 points, respectively. In addition, the chemical composition of the desorbed shale gas was examined using an Agilent7890 B Gas Chromatography (GC) System equipped with two thermal conductivity detectors (TCD) and one flame ionization detector (FID).[20]

A coupled system consisting of an Agilent 7890B gas chromatograph, an Elementar Isoprime Precision isotope mass spectrometer, and an Elementar GC5 pyrolyzer determined the carbon isotope composition of the desorbed gases. Split injection mode was used in this system with a split ratio of 1:3 and an injection temperature of 300 °C. The gas components

https://doi.org/10.1021/acsomega.3c08330
ACS Omega 2024, 9, 13764−13781

were separated by a PLOT-Q column (30 m × 0.32 mm × 20 μm) and carried by He gas at a 1.2 mL/min constant flow rate. The gases were converted to CO_2 in a furnace set at 940 °C. The oven temperature was initially fixed at 40 °C for 6 min before it was elevated to 150 °C at a heating rate of 30 °C/min and held for 1 min. Vienna Pee Dee Belemnite (VPDB) standard calibrated the system. The measurement precision was ±0.5‰ for $\delta^{13}C$.

3. RESULTS AND DISCUSSION

3.1. Geochemical Characteristics of Shale Samples. The LCNF shales of the the SZY1 well have an average total organic carbon (TOC) content of 4.31% (range = 2.78−8.35%). The average $S_1 + S_2$ ranged from 0.08 to 0.24 mg/g (Table 1) and was high over maturity with a vitrinite equivalent reflectance (R_{equiv}) range of 2.44−2.78%. The R_{equiv} is based on the bitumen reflectance (R_b) equation proposed by previous researchers[55] (Table 1). The R_{equiv} values agree with the Niutitang shales (1.51−3.19%) reported for the outcrop samples from the Micangshan Tectonic zone.[50] Additionally, maceral analysis of shale core samples indicated the LCNF shale of the study area is classified as type I kerogen (Table 1), a good gas source because the oils cracked to wet gas when R_o is >1.4%. In comparison, all condensate-rich gases cracked to dry gas when R_o is >2.0%.[56]

3.2. Gas-Bearing Properties of Shale. In situ gas desorption experiments examined the desorbed gas from nine shale core samples collected from the LCNF of the SZY1 Well. Based on the method established by USBM (1973), the scattered or disappeared gas constituents lost between core drilling and core canister sealing were as tagged as lost gas. Also, at the end of the desorption, the gas reserved in the disconnected pores could be released by desorption. Hence, it was termed residual gas; it is negligible. Consequently, the desorbed gas and lost gas were considered when the total gas content.

The mean (range) of the desorbed gas and total gas contents of the nine shale samples were 1.45 (0.95−2.50) and 2.30 (1.34−3.81) cm^3/g, respectively (Table 1). According to the evaluation criteria for the gas content of LCNF shale suggested by a previous study,[49] five shale samples belonged to the gas-rich shale category while the other four were high-gas shale, indicating LCNF in south Shanxi is the favorable stratum for exploration. Figure 3 shows a strong positive linear correlation between desorbed gas content and TOC (2.78−8.35%), a common phenomenon already reported.[8,59]

3.3. Adsorbability of the Shale Toward Various Gases. *3.3.1. Constituents of the Desorbed Gases.* The 169 gas samples obtained from the desorption phases were analyzed by GC. Air mixing with shale gas is unavoidable during the desorption experiment (Li et al., 2021). Figure 4 shows that the N_2 content correlated positively with the O_2 content, and N_2/O_2 (mean of 2.33) varies between 1.89 and 3.45, lower than the 3.72 found in the air. Based on N_2/O_2, N_2 was completely removed, while some of the O_2 content was retained. However, previous studies reported that no O_2 exists in the LCNF shale gas.[5,8,9,25] Therefore, N_2 and O_2 were removed in this study, normalizing the remaining gases to 100% (Table 2).

The desorbed gas consisted of large and small amounts of hydrocarbon and nonhydrocarbon gases, respectively. Hydrocarbon gases consisted of CH_4, C_2H_6 and very little C_3H_8 which only existed in SZY1−3 and SZY1−4 core samples

Table 1. Basic Geochemical Data of the Shale Sample and Testing Results of Desorbed Shale Gas[a]

sample ID	depth (m)	TOC/%	$S_1 + S_2$/ (mg/g)	R_b/%	R_{equiv}/%	desorbed gas content (cm^3/g)	total gas content (cm^3/g)	kerogen type	$\delta^{13}C_{1F}$/‰	$\delta^{13}C_{2F}$/‰	$\delta^{13}C_{1L}$/‰	$\delta^{13}C_{2L}$/‰	$\delta^{13}C_{1L2}$/‰
SZY1−1	1950.74−1951.00	3.20	0.10	3.34	2.59	1.13	2.55	I	−28.90	−37.29	−16.78	−33.87	−16.78
SZY1−2	1962.03−1962.31	2.78	0.12	3.42	2.64	0.95	1.34	I	−30.19	−37.53	−21.63	−33.40	−24.15
SZY1−3	1970.38−1970.64	8.35	0.24	3.28	2.55	2.27	3.49	I	−29.79	−37.78	−4.00	−32.17	−8.07
SZY1−4	1979.36−1979.61	6.81	0.18	3.18	2.48	2.50	3.81	I	−33.41	−37.41	−1.45	−33.17	−5.62
SZY1−5	1990.22−1990.49	2.95	0.08	3.28	2.55	1.02	1.47	I	−31.74	−38.51	−10.87	−32.01	−14.15
SZY1−6	2000.67−2000.87	4.17	0.11	3.41	2.64	1.50	2.48	I	−25.73	−37.53	−1.82	−32.71	−5.61
SZY1−7	2009.91−2010.19	3.46	0.09	3.13	2.44	1.03	1.57	I	−32.89	−38.19	−2.97	−32.31	−11.30
SZY1−8	2014.86−2015.14	2.97	0.09	3.53	2.72	1.19	1.77	I	−31.93	−36.26	−5.27	−33.92	−12.98
SZY1−9	2023.61−2023.89	4.12	0.12	3.63	2.78	1.50	2.22	I	−30.92	−38.44	−6.89	−33.82	−14.06

[a] $\delta^{13}C_{1F}$ = the value of $\delta^{13}C_1$ of the first desorbed shale gas sample, $\delta^{13}C_{2F}$ = the value of $\delta^{13}C_2$ of the first desorbed shale gas sample, $\delta^{13}C_{1L}$ = the value of $\delta^{13}C_1$ of the last desorbed shale gas sample, $\delta^{13}C_{2L}$ = the value of $\delta^{13}C_2$ of the last desorbed shale gas sample, $\delta^{13}C_{1L2}$ = = the value of $\delta^{13}C_1$ of desorbed shale gas sample with desorbed time of about 21 h.

https://doi.org/10.1021/acsomega.3c08330
ACS Omega 2024, 9, 13764−13781

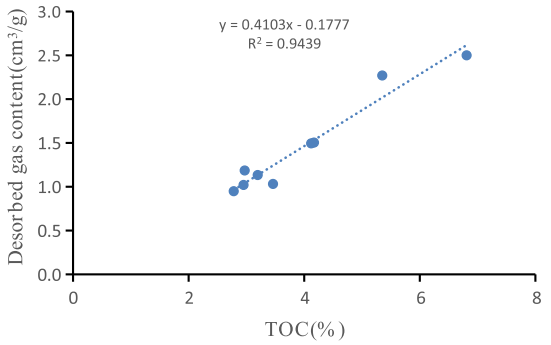

Figure 3. Crossplot of desorbed shale gas content versus TOC of shale core samples.

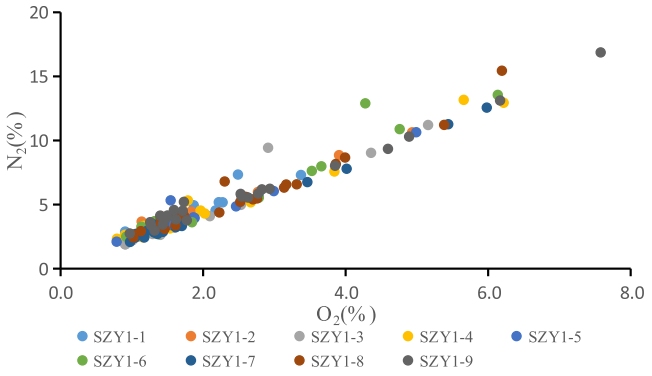

Figure 4. Crossplot of N_2 and O_2 contents of desorbed shale gas samples.

(Table 2, Figure 5e), whereas nonhydrocarbon gases consisted of H_2, CO_2 and very little He which was only detected in the SZY1−2 core sample (Table 2, Figure 5f).

CH_4 was the predominant hydrocarbon gas. Herein, the average (range) CH_4 content of the first and last desorbed gas from the shale core samples were 98.18% (97.33−98.48%) and 88.38% (82.06−94.59%), respectively (Table 2, Figure 5a). Compared with the CH_4 content, the C_2H_6 content was relatively low. The average (range) C_2H_6 content of the first and last desorbed gas were 1.51% (1.17−2.49%) and 7.37% (2.56−11.76%), respectively (Table 2, Figure 5b). Thus, unlike C_2H_6, CH_4 exhibited a lowering trend (Figure 5a-b), suggesting a different adsorbability of CH_4 and C_2H_6 onto the shale core. Additionally, C_3H_8 was the other hydrocarbon identified.

The nonhydrocarbon gases were H_2, CO_2, and He. The mean (range) CO_2 content of the first and last desorbed gases were 0.03% (0.02−0.04%) and 0.21% (0.11−0.47%), respectively (Table 2, Figure 5c). At phase I of desorption, H_2 was present in trace amounts (0.004−0.04%), while H_2 increased to 0.67−3.07% at phase III of desorption (Table 2, Figure 5d). In general, the quantity of these two gases increased as desorption proceeded, albeit at different growth rates. In addition, He existed negligibly in phase I of desorption of the SZY1−2 sample. Hence, He was undetected in the other gas samples (Table 2, Figure 5f). Nevertheless, the He content decreased as desorption progressed, indicating that the gas has an adsorption pattern different from that of H_2 and CO_2.

In addition, the methane content dropped continuously during desorption, lowering the mean (range) dryness index (C_1/C_{1-5}) from 98.48% (97.50−98.82%) from the first desorbed gas to 92.26% (87.46−97.36%) of the last desorbed gas samples. However, given the overall CH_4 proportion in the desorbed gas, the shale gas produced from the LCNF in MTZSS is a typical dry gas (Table 2, Figure 6).

3.3.2. Gas Adsorbability Sequence of Shale. Figure 5a shows that CH_4 content was relatively stable, albeit showing a steady fall in Phases I and II with a constant desorption temperature. In contrast, a dramatic decrease in Phase III occurred. Contrarily, C_2H_6, CO_2, and H_2 contents were relatively stable with a steady rise in Phases I and II, while Phase III exhibited a significantly rising profile (Figure 5b−d). C_2H_6, CO_2, and H_2 contents maintained a rising trend in Phase III of the desorption. Nevertheless, C_2H_6, CO_2, and H_2 accounted for a minute proportion of shale gases relative to CH_4. Therefore, it is strongly suggested that the residue gas is predominantly CH_4.

Furthermore, Figure 5d,f illustrate how fast He was quickly desorbed in phases I and II, while the respective H_2 amounts desorbed were negligible and minute, such as in SZY1−1, SZY1−2, SZY1−8, and SZY1−9 core samples. It is opined that the deciphered shale has a weak capacity to adsorb He but a strong capacity toward H_2. In addition, the C_3H_8 content did not change with increasing desorption temperature, probably owing to its minimal content (Table 2, Figure 5e).

Adsorption leads to increasing shale gas storage capacity by two or more times than without adsorption.[60] van der Waals forces exist between shale (adsorbent) and shale gas (an adsorbate). Hence, the shale gas adsorption onto the shale is via reversible physisorption.[61] Therefore, adsorption is an exothermic process,[62] whereas desorption is endothermic. One of the fundamental properties of gas molecules is the existence of intermolecular forces among them, mainly derived from electrostatic forces. The intermolecular forces cause a multilayer gas accumulation,[63] forming a high-density adsorbed phase different from the free counterpart.[64] In addition, higher pressure made it easier to form a multilayer of gas accumulation.[65] Overall, the shale gas accumulation depends on the temperature, pressure, and properties of the adsorbate (shale gas) and adsorbent (shale).

In Phase I of desorption, the gases with weak adsorbability were desorbed faster than the gases with strong adsorbability. Hence, the content of the former (such as CH_4 and He) decreased gently with desorption while those of the latter (such as C_2H_6, CO_2, and H_2) increased gradually during desorption. Figure 7a−d illustrate a significant negative correlation between the CH_4 content and those of C_2H_6, CO_2, and H_2. Also, the CH_4 content correlates positively with the He content, indicating similar affinities of shale toward CH_4 and He, but different for C_2H_6, CO_2, and H_2.

Based on the relationship between adsorbability and desorption rate and the variations in gas ratios with desorbed time and temperature, the sequence of adsorbability of the shale toward the gases was confirmed (Figures 8a−d). H_2/CO_2, C_2H_6/CH_4, and CH_4/He ratios had a generally rising trend with increasing desorbed time and temperature (Figures 8a−c), demonstrating that the adsorbability of the shale toward H_2 is stronger than that for CO_2 and O_2. The shale's adsorbability was C_2H_6 > CH_4 > He. As for CO_2/C_2H_6, this ratio remained relatively steady at phases I and II before it slowly increased at phase III (Figure 8d). Such a trend shows that the sequence of adsorbability for CO_2 and C_2H_6 was similar in phases I and II, while the counterpart was CO_2 > C_2H_6 in phase III.

https://doi.org/10.1021/acsomega.3c08330
ACS Omega 2024, 9, 13764−13781

Table 2. Geochemical Characteristics of Shale Gases Derived from the In Situ Desorption Experiments of the Niutitang Formation Shale of the SZY1 Well

core sample ID	gas sample ID	sampling time (h)	main component (vol, %)										$\delta^{13}C_{PDB}$ (‰)	
			He	H_2	CH_4	C_2H_6	CO_2	C_3H_8	C_1/C_{1-5}	$C_1/(C_2 + C_3)$	$\ln(C_1/C_2)$	$\ln(C_2/C_3)$	CH_4	C_2H_6
SZY1−1	1	0.53		0.01	97.45	2.50	0.04		97.50	39.02	3.66		−28.90	−37.29
	2	1.69		0.04	97.22	2.67	0.07		97.33	36.47	3.60		−26.77	−36.25
	3	2.83		0.06	97.28	2.59	0.07		97.41	37.54	3.63		−25.78	−36.48
	4	3.85		0.07	97.40	2.45	0.08		97.55	39.76	3.68		−23.55	−35.12
	5	4.94		0.08	97.31	2.51	0.10		97.49	38.78	3.66		−24.58	−35.83
	6	6.34		0.10	97.20	2.62	0.09		97.38	37.15	3.61		−24.08	−35.80
	7	8.31		0.12	97.19	2.59	0.10		97.40	37.46	3.62		−22.57	−34.30
	8	11.39		0.16	97.09	2.65	0.11		97.35	36.68	3.60		−21.12	−34.79
	9	14.38		0.20	96.28	3.31	0.21		96.68	29.08	3.37		−18.64	−35.02
	10	17.14		0.46	93.96	5.12	0.45		94.83	18.34	2.91		−17.70	−36.48
	11	20.94		0.83	93.69	5.01	0.47		94.92	18.70	2.93		−16.78	−33.87
SZY1−2	1	0.48	0.03	0.03	98.47	1.44	0.03		98.56	68.33	4.22		−30.19	−37.53
	2	1.60	0.03	0.02	98.55	1.36	0.03		98.64	72.36	4.28		−29.36	−36.09
	3	2.87	0.02	0.02	98.59	1.33	0.03		98.67	74.22	4.31		−30.26	
	4	3.93	0.02	0.02	98.10	1.84	0.03		98.16	53.42	3.98		−21.72	
	5	4.81	0.01	0.03	97.61	2.30	0.03		97.69	42.37	3.75		−28.18	−36.50
	6	5.89	0.01	0.05	97.69	2.20	0.04		97.80	44.36	3.79		−27.83	−34.92
	7	7.11	0.01	0.07	97.70	2.19	0.04		97.81	44.67	3.80		−27.29	−34.83
	8	8.43	0.01	0.08	97.97	1.89	0.05		98.10	51.76	3.95		−25.34	−33.77
	9	10.22	0.01	0.09	97.75	2.11	0.04		97.89	46.28	3.83		−26.62	−35.71
	10	12.46	0.01	0.12	97.70	2.15	0.03		97.84	45.40	3.82		−26.20	−36.60
	11	14.48		0.17	96.72	3.07	0.04		96.93	31.55	3.45		−25.81	−35.12
	12	16.52		0.34	96.05	3.54	0.07		96.45	27.14	3.30		−25.06	−35.13
	13	19.47		0.47	96.32	3.13	0.08		96.85	30.78	3.43		−24.15	−33.96
	14	22.25		0.54	96.59	2.78	0.09		97.20	34.76	3.55		−25.10	−33.94
	15	26.92		0.60	96.09	3.20	0.10		96.77	30.00	3.40		−23.04	−33.58
	16	36.03		0.67	96.60	2.62	0.12		97.36	36.91	3.61		−21.63	−33.40
SZY1−3	1	0.01		0.02	98.65	1.30	0.03		98.69	75.60	4.33		−29.79	−37.78
	2	0.48		0.00	98.33	1.65	0.02		98.35	59.67	4.09		−30.46	−36.99
	3	1.44		0.01	98.16	1.81	0.03		98.19	54.36	4.00		−28.70	−36.98
	4	2.20		0.01	98.10	1.87	0.02		98.13	52.39	3.96		−26.42	−35.06
	5	2.88		0.01	98.13	1.83	0.03		98.17	53.69	3.98		−24.00	−34.56
	6	3.66		0.01	97.48	2.49	0.02		97.51	39.19	3.67		−25.94	−35.45
	7	4.37		0.05	95.75	4.15	0.02	0.03	95.82	22.92	3.14	5.07	−23.80	−35.35
	8	5.23		0.13	95.13	4.67	0.02	0.04	95.28	20.18	3.01	4.75		
	9	5.54		0.13	95.13	4.67	0.02	0.04	95.28	20.18	3.01	4.75		
	10	6.23		0.21	95.24	4.49	0.03	0.04	95.46	21.03	3.05	4.82	−19.94	−35.48
	11	7.28		0.27	95.27	4.40	0.03	0.03	95.56	21.51	3.08	4.90	−18.26	−35.33
	12	8.33		0.31	95.27	4.35	0.03	0.03	95.60	21.75	3.09	4.99	−16.73	−36.57
	13	9.48		0.37	94.99	4.57	0.03	0.04	95.37	20.60	3.03	4.81	−17.52	−35.61
	14	11.07		0.46	94.84	4.64	0.03	0.04	95.30	20.28	3.02	4.82	−16.34	−35.26
	15	13.08		0.58	94.67	4.69	0.03	0.04	95.25	20.05	3.01	4.87	−14.23	−34.91
	16	14.50		0.61	93.27	6.02	0.04	0.07	93.87	15.32	2.74	4.47	−14.23	−35.31
	17	15.44		0.78	90.61	8.43	0.05	0.13	91.37	10.59	2.37	4.19	−13.01	−35.06
	18	17.33		1.68	88.86	9.25	0.07	0.14	90.44	9.46	2.26	4.17	−10.85	−34.71
	19	22.45		2.17	88.09	9.50	0.09	0.14	90.13	9.13	2.23	4.19	−8.07	−33.67
	20	29.73		2.53	88.13	9.10	0.11	0.13	90.53	9.56	2.27	4.28	−6.22	−33.09
	21	35.64		2.72	87.94	9.10	0.13	0.10	90.53	9.56	2.27	4.47	−4.00	−32.17
SZY1−4	1	0.13		0.00	98.36	1.61	0.02		98.39	60.94	4.11		−33.41	−37.41
	2	0.52		0.00	98.17	1.79	0.03		98.21	54.73	4.00		−40.91	
	3	1.05		0.01	97.99	1.98	0.02		98.02	49.48	3.90		−31.17	−38.14
	4	1.60		0.01	98.00	1.97	0.02		98.03	49.76	3.91		−27.55	−37.11
	5	2.10		0.01	98.12	1.85	0.03		98.15	53.10	3.97		−28.54	−36.89
	6	2.65		0.01	98.04	1.92	0.03		98.08	50.99	3.93		−27.96	−37.84
	7	3.31		0.01	98.23	1.72	0.04		98.28	57.20	4.05		−26.73	−37.73
	8	3.98		0.03	96.64	3.30	0.03		96.70	29.32	3.38		−25.11	−36.57
	9	4.70		0.11	95.20	4.64	0.04		95.35	20.50	3.02		−22.39	−36.51
	10	5.67		0.22	95.10	4.63	0.05		95.36	20.54	3.02		−22.07	−38.34
	11	6.70		0.27	95.08	4.56	0.05	0.05	95.38	20.64	3.04	4.61	−19.23	−37.17
	12	7.75		0.33	95.25	4.36	0.05		95.62	21.86	3.08		−14.59	−35.54

https://doi.org/10.1021/acsomega.3c08330
ACS Omega 2024, 9, 13764−13781

Table 2. continued

core sample ID	gas sample ID	sampling time (h)	main component (vol, %)										$\delta^{13}C_{PDB}$ (‰)	
			He	H_2	CH_4	C_2H_6	CO_2	C_3H_8	C_1/C_{1-5}	$C_1/(C_2 + C_3)$	$\ln(C_1/C_2)$	$\ln(C_2/C_3)$	CH_4	C_2H_6
	13	8.91		0.38	95.01	4.56	0.05		95.42	20.84	3.04		−14.36	−35.31
	14	10.22		0.45	94.87	4.59	0.05	0.04	95.35	20.49	3.03	4.71	−17.55	
	15	12.09		0.55	94.79	4.56	0.06	0.04	95.37	20.62	3.03	4.77	−12.84	−35.81
	16	13.95		0.66	93.85	5.43	0.06		94.53	17.27	2.85		−11.48	−35.76
	17	15.36		0.84	90.93	8.12	0.12		91.80	11.20	2.42		−10.58	−35.01
	18	17.43		1.57	88.25	10.02	0.16		89.81	8.81	2.18		−9.21	−35.34
	19	22.34		2.22	88.02	9.58	0.18		90.18	9.19	2.22		−5.62	−35.42
	20	32.45		2.42	89.19	8.21	0.19		91.58	10.87	2.39		−2.62	−33.39
	21	34.95		2.64	86.44	10.59	0.33		89.08	8.16	2.10		−1.55	−32.66
	22	41.90		3.07	84.38	12.10	0.46		87.46	6.98	1.94		−1.45	−33.17
SZY1−5	1	0.28		0.02	98.14	1.82	0.02		98.18	53.89	3.99		−31.74	−38.51
	2	0.98		0.01	98.09	1.87	0.02		98.13	52.38	3.96		−30.26	−35.72
	3	2.02		0.02	98.09	1.87	0.02		98.13	52.37	3.96		−28.40	−36.39
	4	3.17		0.02	98.06	1.89	0.03		98.11	51.96	3.95		−27.68	−35.82
	5	4.15		0.04	96.65	3.29	0.02		96.71	29.41	3.38		−27.39	−36.60
	6	5.09		0.16	95.99	3.82	0.03		96.18	25.15	3.22		−25.02	−35.69
	7	6.16		0.23	95.69	4.06	0.02		95.93	23.57	3.16		−24.06	−35.65
	8	7.25		0.30	95.59	4.09	0.02		95.90	23.39	3.15		−22.89	−35.01
	9	8.67		0.38	95.65	3.94	0.03		96.04	24.26	3.19		−21.82	−35.38
	10	11.03		0.45	95.69	3.82	0.04		96.16	25.06	3.22		−19.65	−34.59
	11	14.64		0.52	95.83	3.61	0.04		96.37	26.55	3.28		−18.36	−34.97
	12	15.78		0.61	93.97	5.37	0.05		94.60	17.51	2.86		−17.08	−34.17
	13	17.79		1.04	92.07	6.83	0.07		93.10	13.49	2.60		−15.97	−33.86
	14	21.07		1.37	90.94	7.61	0.08		92.28	11.95	2.48		−14.15	−33.84
	15	35.21		1.46	91.96	6.46	0.11		93.43	14.23	2.66		−10.87	−32.01
SZY1−6	1	0.22		0.00	98.73	1.24	0.02		98.76	79.51	4.38		−25.73	−37.53
	2	0.68		0.01	98.51	1.45	0.02		98.55	67.73	4.22		−29.84	−36.98
	3	1.32		0.00	98.37	1.61	0.02		98.39	61.28	4.12		−28.15	−34.90
	4	2.05		0.01	98.41	1.56	0.03		98.44	63.11	4.14		−25.51	−36.95
	5	2.73		0.01	98.48	1.47	0.04		98.53	67.05	4.21		−23.97	−36.55
	6	3.45		0.01	97.90	2.06	0.03		97.94	47.47	3.86		−24.05	−35.61
	7	4.51		0.11	95.67	4.18	0.04		95.81	22.87	3.13		−19.59	−34.80
	8	5.85		0.19	95.45	4.32	0.03		95.67	22.09	3.10		−18.54	−34.87
	9	7.92		0.30	95.46	4.20	0.04		95.79	22.74	3.12		−14.85	−34.56
	10	12.10		0.45	95.61	3.89	0.06		96.09	24.59	3.20		−12.00	−34.27
	11	14.41		0.62	94.99	4.32	0.07		95.65	22.00	3.09		−8.65	−33.67
	12	15.78		0.75	91.71	7.47	0.07		92.47	12.28	2.51		−8.26	−33.51
	13	19.20		1.36	90.08	8.47	0.10		91.41	10.64	2.36		−5.61	−33.19
	14	33.80		2.30	88.65	8.93	0.12		90.85	9.93	2.30		−1.82	−32.71
SZY1−7	1	0.28		0.01	98.71	1.25	0.03		98.75	78.91	4.37		−32.89	−38.19
	2	0.85		0.01	98.48	1.49	0.02		98.51	66.17	4.19		−30.84	−37.09
	3	1.37		0.01	98.45	1.52	0.02		98.48	64.67	4.17		−28.58	−35.88
	4	2.07		0.01	98.44	1.53	0.03		98.47	64.40	4.17		−28.50	−36.95
	5	3.29		0.01	98.42	1.53	0.03		98.46	64.12	4.16		−26.37	−37.22
	6	4.23		0.02	98.18	1.78	0.03		98.22	55.15	4.01		−26.38	−36.80
	7	4.61		0.02	97.30	2.66	0.02		97.34	36.64	3.60		−25.67	−36.11
	8	4.99		0.05	96.67	3.25	0.03		96.75	29.77	3.39		−25.77	−36.53
	9	5.49		0.10	96.11	3.77	0.02		96.23	25.50	3.24		−24.57	−36.98
	10	6.20		0.16	96.15	3.66	0.03		96.34	26.31	3.27		−22.86	−34.62
	11	7.23		0.22	95.93	3.83	0.03		96.17	25.08	3.22		−21.25	−34.55
	12	8.80		0.29	95.87	3.80	0.03		96.18	25.20	3.23		−19.39	−35.57
	13	11.35		0.39	95.71	3.87	0.03		96.12	24.75	3.21		−17.05	−35.95
	14	14.10		0.51	94.83	4.63	0.04		95.34	20.48	3.02		−15.61	−35.03
	15	16.43		0.77	91.99	7.19	0.05		92.75	12.80	2.55		−14.55	−35.29
	16	19.65		1.34	92.09	6.50	0.08		93.41	14.17	2.65		−11.30	−33.53
	17	24.76		1.61	90.73	7.59	0.08		92.28	11.96	2.48		−9.58	−34.36
	18	36.43		1.91	91.14	6.85	0.09		93.01	13.31	2.59		−5.61	−32.68
	19	45.90		2.13	89.22	8.48	0.17		91.32	10.52	2.35		−2.97	−32.31
SZY1−8	1	0.11		0.04	98.75	1.18	0.03		98.82	83.75	4.43		−31.93	
	2	0.36		0.01	98.89	1.09	0.02		98.91	91.11	4.51		−31.27	
	3	0.56		0.01	98.82	1.15	0.02		98.85	85.82	4.45		−31.80	

https://doi.org/10.1021/acsomega.3c08330
ACS Omega 2024, 9, 13764−13781

Table 2. continued

core sample ID	gas sample ID	sampling time (h)	main component (vol, %)										$\delta^{13}C_{PDB}$ (‰)	
			He	H_2	CH_4	C_2H_6	CO_2	C_3H_8	C_1/C_{1-5}	$C_1/(C_2+C_3)$	$\ln(C_1/C_2)$	$\ln(C_2/C_3)$	CH_4	C_2H_6
	4	0.83		0.00	98.73	1.24	0.02		98.76	79.37	4.37		−31.00	
	5	1.21		0.00	98.68	1.29	0.02		98.71	76.32	4.33		−30.08	
	6	1.78		0.00	98.69	1.28	0.03		98.72	77.00	4.34			
	7	2.76		0.00	98.60	1.38	0.02		98.62	71.65	4.27		−27.58	−36.26
	8	3.64		0.01	98.29	1.68	0.02		98.32	58.36	4.07		−25.93	−39.75
	9	4.14		0.01	97.51	2.46	0.02		97.54	39.66	3.68		−26.88	−36.46
	10	4.70		0.03	96.99	2.96	0.02		97.04	32.81	3.49		−26.30	−37.56
	11	5.55		0.05	96.96	2.96	0.03		97.03	32.71	3.49			
	12	6.59		0.06	96.98	2.93	0.03		97.07	33.14	3.50		−22.77	−36.40
	13	7.89		0.09	96.82	3.07	0.03		96.93	31.57	3.45		−21.80	−36.85
	14	9.67		0.11	97.12	2.74	0.04		97.26	35.46	3.57		−19.70	−36.40
	15	11.29		0.13	97.36	2.47	0.05		97.53	39.49	3.68		−18.92	−35.48
	16	12.56		0.15	97.00	2.81	0.05		97.19	34.56	3.54		−18.55	−36.59
	17	14.26		0.18	96.94	2.83	0.05		97.17	34.31	3.54		−17.43	−36.04
	18	14.79		0.20	96.19	3.56	0.05		96.43	27.03	3.30		−17.25	−35.75
	19	15.54		0.23	94.99	4.73	0.05		95.26	20.10	3.00		−17.11	−35.40
	20	16.71		0.37	94.51	5.05	0.07		94.93	18.71	2.93		−16.02	−35.01
	21	18.56		0.59	93.59	5.75	0.07		94.21	16.28	2.79		−15.06	−35.27
	22	21.39		0.82	93.63	5.47	0.08		94.48	17.13	2.84		−12.98	−35.42
	23	27.42		1.01	92.88	6.02	0.09		93.91	15.42	2.74		−11.24	−35.19
	24	34.96		1.25	93.02	5.63	0.10		94.30	16.53	2.81		−8.35	−34.57
	25	41.76		1.42	91.25	7.16	0.17		92.73	12.75	2.55		−5.27	−33.92
SZY1−9	1	0.17		0.01	98.68	1.28	0.02		98.71	76.82	4.34		−30.92	−38.44
	2	0.63		0.01	98.38	1.59	0.02		98.41	61.93	4.13		−29.37	−38.72
	3	1.13		0.01	98.34	1.63	0.02		98.37	60.26	4.10		−28.32	
	4	1.61		0.01	98.31	1.66	0.02		98.34	59.23	4.08		−29.14	−38.40
	5	2.28		0.01	98.34	1.63	0.02		98.37	60.34	4.10		−28.18	−38.25
	6	3.18		0.01	98.38	1.59	0.03		98.41	61.91	4.13		−26.77	−37.43
	7	3.97		0.01	96.89	3.08	0.02		96.92	31.47	3.45		−26.05	−38.09
	8	4.65		0.04	95.99	3.95	0.02		96.05	24.29	3.19		−26.14	−38.40
	9	5.52		0.05	96.15	3.77	0.03		96.23	25.49	3.24		−24.85	−37.67
	10	6.62		0.06	96.24	3.67	0.03		96.33	26.25	3.27		−19.72	−37.01
	11	7.86		0.07	96.34	3.56	0.03		96.43	27.04	3.30		−22.77	−37.33
	12	9.27		0.09	96.38	3.50	0.03		96.49	27.50	3.31		−21.13	−37.68
	13	11.18		0.10	96.79	3.07	0.04		96.93	31.54	3.45		−19.23	−36.48
	14	12.33		0.11	96.57	3.29	0.04		96.71	29.39	3.38		−20.12	−36.79
	15	13.80		0.12	96.55	3.28	0.04		96.71	29.41	3.38		−19.12	−36.53
	16	14.41		0.14	94.90	4.93	0.03		95.06	19.24	2.96		−17.97	−37.38
	17	16.08		0.31	92.94	6.71	0.04		93.26	13.84	2.63		−16.60	−36.68
	18	18.63		0.45	93.10	6.39	0.06		93.58	14.57	2.68		−15.40	−36.31
	19	20.67		0.51	93.10	6.33	0.06		93.63	14.70	2.69		−14.06	−36.08
	20	23.23		0.55	93.05	6.33	0.07		93.63	14.69	2.69		−13.12	−36.04
	21	27.00		0.60	93.54	5.79	0.07		94.17	16.15	2.78		−17.52	
	22	32.73		0.65	93.79	5.47	0.08		94.49	17.14	2.84		−10.64	−35.21
	23	48.25		0.70	92.58	6.62	0.11		93.33	13.98	2.64		−8.23	−35.03
	24	59.43		1.05	90.80	8.00	0.15		91.90	11.34	2.43		−6.89	−33.82

Moreover, the C_3H_8 content was limited, and the variation trend of its ratios to those of the other gases was irregular. Therefore, the sequence of adsorbability of the shale to different gases was $H_2 > CO_2 > C_2H_6 > CH_4 >$ He, which was almost consistent with previous conclusions.[20,25] The order of absorption capacity of the shale from the Upper Ordovician Wufeng Formation-Lower Silurian Longmaxi Formation in west Hubei for different gas components is determined to be $CO_2 > H_2 > C_3H_8 > C_2H_6 > CH_4 >$ He. Furthermore, CO_2 and C_2H_6 have higher adsorption affinities to the organic shales from the Lower Silurian Longmaxi Formation and the Lower Cambrian Shuijingtuo Formation in the eastern part of Chongqing than CH_4, causing early desorbed gases to be relatively enriched in CH_4, whereas gases desorbed later are relatively enriched in CO_2 and C_2H_6, indicating the gas adsorbability sequence of shale was dominated by the varying molecular sizes of gas, which led to the differences of intermolecular forces. Especially for hydrocarbon gases, the accumulation of gas with big molecular size resulting in formation of a high-density adsorbed phase[64] owing to the higher intermolecular forces.

The TOC variation influenced the shale's adsorbability to gaseous hydrocarbons (Figure 3). Therefore, more hydrocarbon gas was adsorbed with the increase in the shale's TOC. In addition, the desorbed gas content was inversely proportional to the dryness index of the last desorbed gas of each core

https://doi.org/10.1021/acsomega.3c08330
ACS Omega 2024, 9, 13764−13781

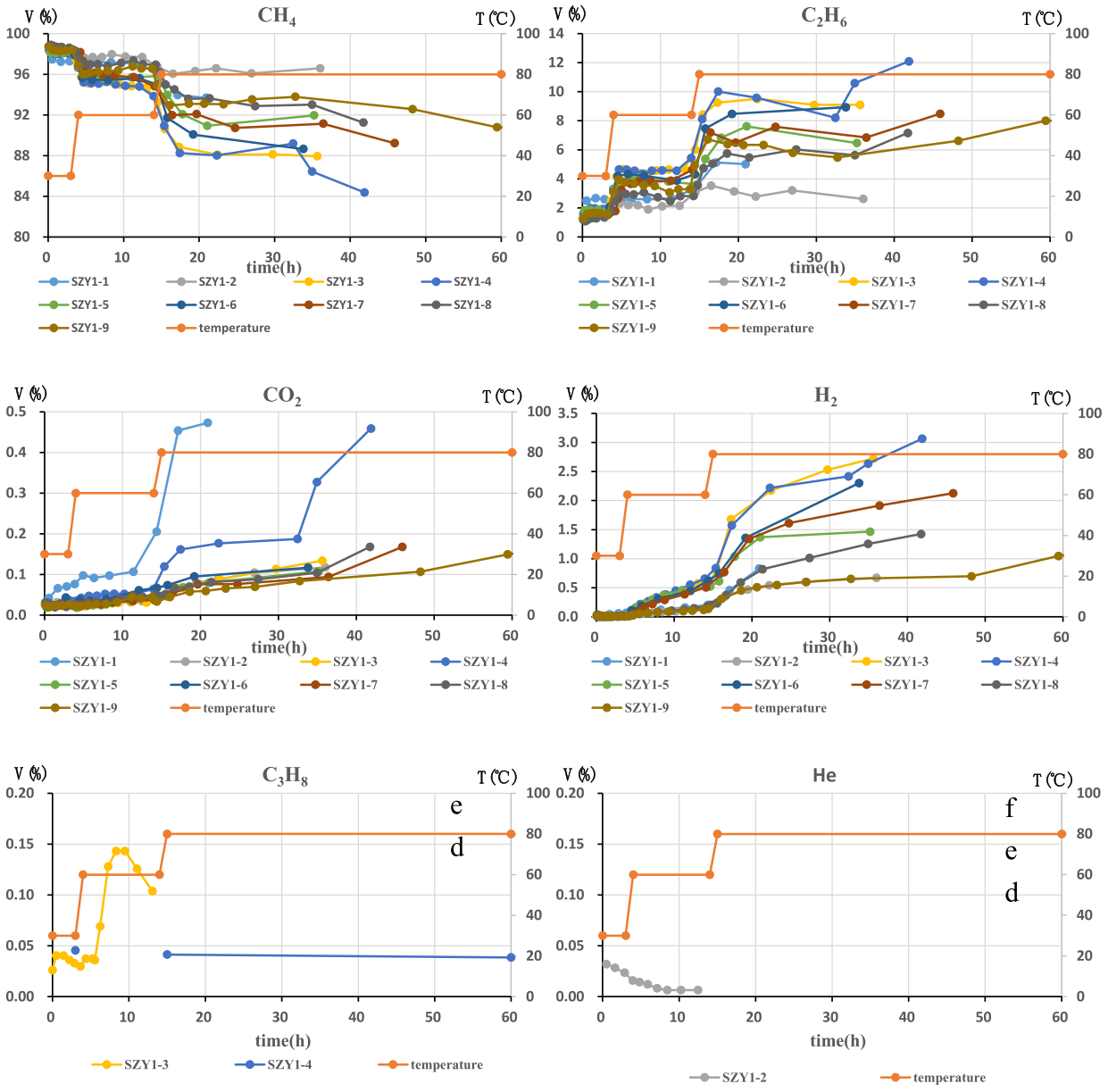

Figure 5. Changes of various gas components with variation of desorbed temperature and time.

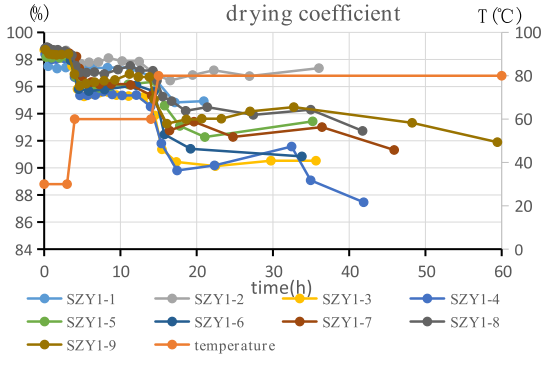

Figure 6. Changes of the dryness index with variation of desrobed temperature and time.

sample (Figure 9a). Hence, the desorbed gas content increases with the decrease in dryness index at the end of desorption.[20,66,67] This phenomenon is thought to be a result of the different adsorbabilities of the shale to gaseous hydrocarbons. The fundamental cause is that the more the shale gas content, the better the reservoir physical properties of shale, with more micropores for enhanced adsorbability.[68] Thus, shale with a higher TOC provides more adsorption space for C_2H_6 and C_3H_8 with relatively stronger adsorbability, leading to more C_2H_6 and C_3H_8 being preserved. As a result, C_2H_6 and C_3H_8 were desorbed in large quantities at the appropriate temperature. However, the desorbed gas content did not correlate with the dryness index of the first desorbed gas of each core sample (Figure 9b) due to the relatively stronger adsorbability. It caused minute amounts of C_2H_6 to be present and C_3H_8 was released at the beginning of desorption. Consequently, the dryness index of the last desorbed gas of the core sample is a useful indicator of sweet spots for shale gas exploration and production.

3.4. Characteristics and Affecting Factors of Carbon Isotope Fractionation during Desorption. *3.4.1. Characteristics of the Carbon Isotope of the Desorbed Gases.* The

https://doi.org/10.1021/acsomega.3c08330
ACS Omega 2024, 9, 13764−13781

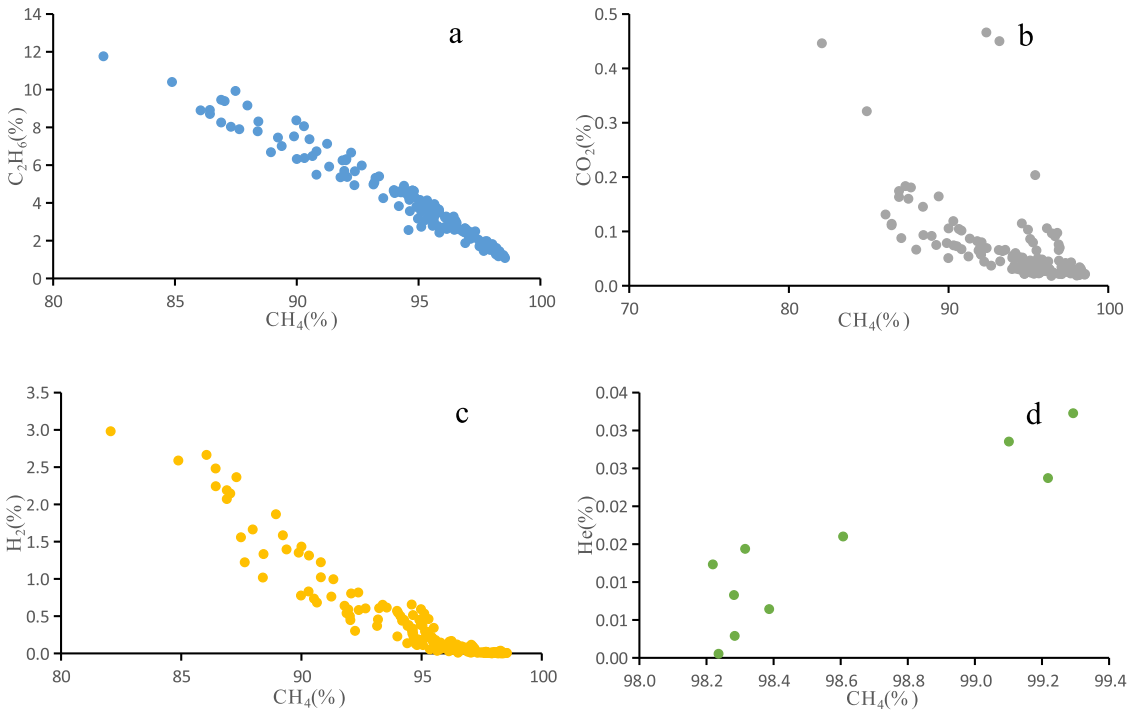

Figure 7. Crossplots of CH_4 contents versus desorbed shale gas samples.

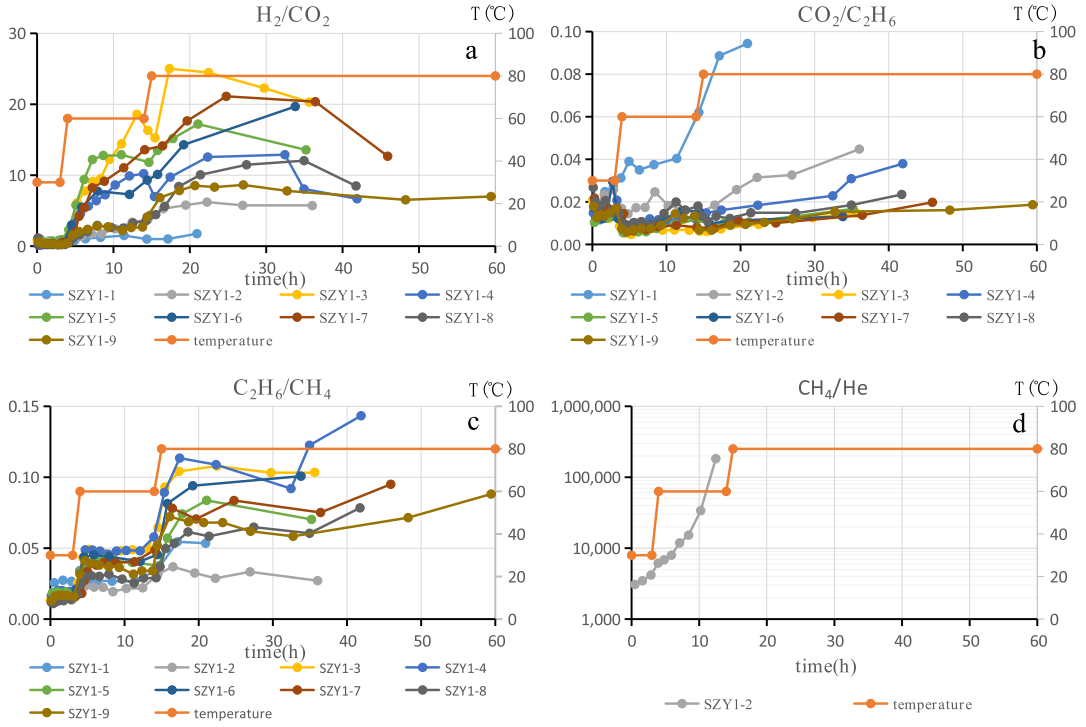

Figure 8. Change of ratios for different gas components of desrobed shale gases with variation of the desorbed temperature and time.

average $\delta^{13}C_1$ (−30.51‰) and $\delta^{13}C_2$ (−37.66‰) values of the first desorbed sample were minimal, ranging between −33.41 and −25.73‰ (Table 1, Figure 10a) and between −38.50 and −36.26‰, (Table 1, Figure 10b), respectively. The $\delta^{13}C_1$ of the desorbed samples gradually increased as the desorption was completed, which is ascribed to the enrichment of $^{13}CH_4$ as desorption proceeded. Overall, the $\delta^{13}C_2$ trend was similar to that of CH_4, with some frequent fluctuations (Table 1, Figure 10a). The value of $\delta^{13}C_1$ of the last desorbed sample varied between −21.63 and −1.45‰ (mean = −7.85‰), while that of $\delta^{13}C_2$ varied narrowly between −33.92 and −32.01‰ (−32.93‰ on average) (Table 1, Figure 10b). The respective overall $\delta^{13}C_1$ and $\delta^{13}C_2$ fractionation of the gases from all core samples were in the range 8.56−31.97‰ and 2.34−6.50‰, with SZY1−4 and SZY1−5 samples exhibiting the highest fractionation degree, respectively (Table 1, Figures 10a, b).

The gases with relatively lighter $\delta^{12}C$ are preferentially released during desorption. Based on this conclusion, two

https://doi.org/10.1021/acsomega.3c08330
ACS Omega 2024, 9, 13764−13781

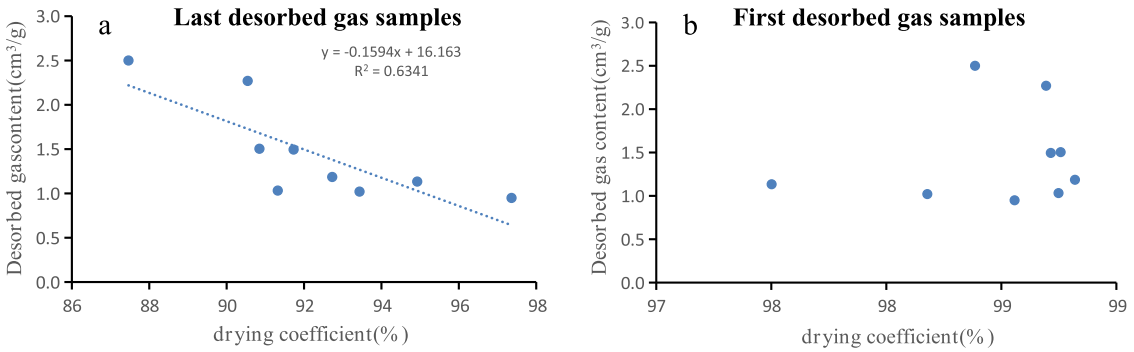

Figure 9. Crossplots of desorbed shale gas content vs dryness index of the last (a) and first desrobed shale gas samples (b).

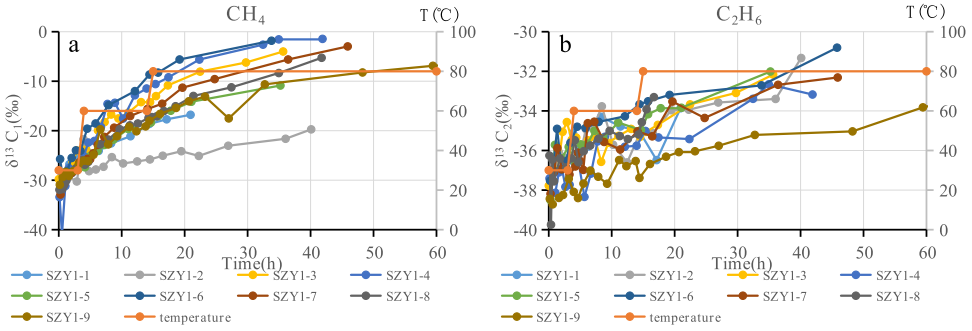

Figure 10. Changes of $\delta^{13}C_1$ and $\delta^{13}C_2$ of desrobed shale gas with variation in desorbed temperature and time.

inferences could be obtained: (i) the $\delta^{13}C$ of the lost shale gas is lighter in comparison with desorbed shale gas; (ii) the shorter the exposure time of the core shale, the lighter the $\delta^{13}C$ at the beginning of desorption (Figure 11). The $\delta^{13}C_1$ of the

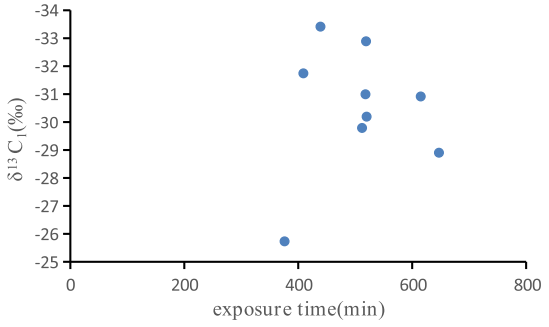

Figure 11. Changes of $\delta^{13}C_1$ of the first desrobed shale gas samples with variation of exposure time referring to time from core drilling to canister sealing of each shale core sample.

first desorbed shale gas of each core sample was inversely proportional to the exposure time of the corresponding sample. Here, the exposure time refers to the time from core drilling to canister sealing. This observation verified the priority of desorption of the relatively lighter $\delta^{12}C$. Therefore, caution should be applied when using the values of $\delta^{13}C$ of hydrocarbon gases, and the desorption phase of the gas sample should be first taken into consideration.

3.4.2. Factors Affecting Carbon Isotope Fractionation. Generally, the gaseous carbon isotopic characteristics ($\delta^{13}C$) of hydrocarbon gases are associated with their genetic source and thermodynamic fractionation. Thus, it commonly serves as an indicator to identify gas sources[26,28,29] and confirm thermal maturity.[69] Thus, carbon isotope fractionation is a highly pervasive phenomenon.[8,20,25,31−34]

The factors influencing carbon isotope fractionation can be classified as internal and external factors. The internal factors (such as TOC and physical properties of shales) intrinsically influence the shale and its gas,[31,32,37] while the external factors are foreign forces. The TOC and the physical properties of shales improve the micropores and nanopores, giving rise to a larger pore volume, and eventually improving the carbon isotope fractionation.[8,33] Furthermore, the volume and proportion of the gases[34,38,70,71] are other internal factors influencing the carbon isotope fractionation. Seepage,[31,72] diffusion,[20,35,72] dissolution,[73] and adsorption/desorption[20,34,38,74] are critical external factors controlling the carbon isotope fractionation. However, determining the most vital factor is still controversial.

Diffusion is a common factor influencing the carbon isotope fractionation of shale gas. It is easily accepted because diffusion usually accompanies desorption during transport or migration.[20] Compared with conventional natural gas, shale gas is an unconventional natural gas characterized by shale as the source rock and reservoir simultaneously. Hence, the shale gas migration distance is much shorter than conventional natural gas, and the carbon isotopic fractionation and composition are not influenced by the effect of migration fractionation.[75,76]

Figure 10a,b shows that $\delta^{13}C_1$ and $\delta^{13}C_2$ gradually became heavier with an increased desorption time. This observation agrees with many research results from the theoretical analyses and simulation experiments.[31,36,71] The value of $\delta^{13}C_2$ decreased slightly in Phases II and III of desorption. In contrast, the value of $\delta^{13}C_1$ was unchanged, growing until the end of desorption, suggesting that the adsorption/desorption was dominant in the carbon isotope fractionation. Diffusion was only significant in the carbon isotope fractionation of the heating phase. In other words, diffusion happened throughout

https://doi.org/10.1021/acsomega.3c08330
ACS Omega 2024, 9, 13764−13781

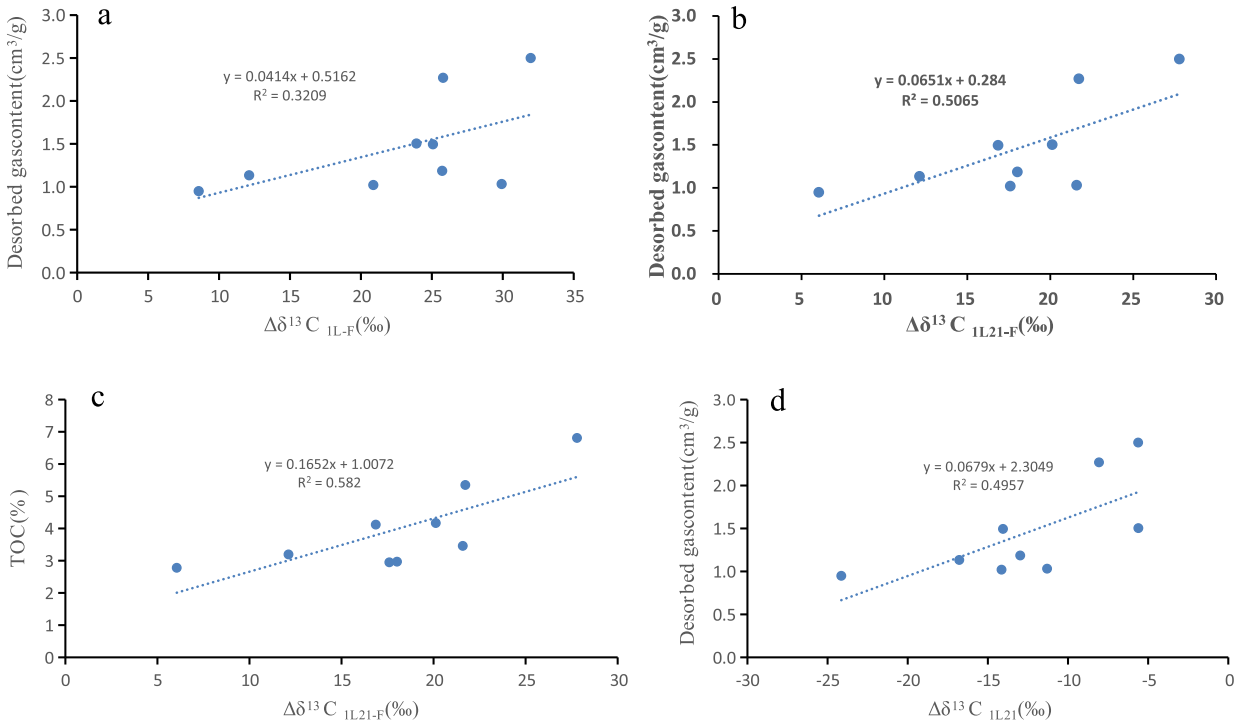

Figure 12. Crossplots of carbon isotope fractionation of CH_4 versus desorbed gas content and TOC (a–c), the value of $\delta^{13}C_1$ of desorbed samples with desorption time of about 21 h ($\delta^{13}C_{1L21}$) versus desorbed gas content. ($\Delta\delta^{13}C_{1L\text{-}F}$ = the difference between the value of $\delta^{13}C_1$ of the last desorbed shale gas sample and that of the first desorbed shale gas sample, $\Delta\delta^{13}C_{1L21\text{-}F}$ = the difference between the value of $\delta^{13}C_1$ of desorbed shale gas sample with desorbed time of about 21 h and that of the first desorbed shale gas sample).

the desorption phases. However, the desorption intensity was much higher than that of diffusion most of the time. Such occurrence was consistent with the above conclusion that the diffusion was limited because the migration distance of shale gas was much shorter than conventional natural gas.

An increase in temperature thermally induces intense diffusion, causing more $^{12}C_2$ to diffuse rapidly through the micropores/nanopores of the shale. Accordingly, $^{12}C_2H_6$ diffusion was sensitive to the temperature increase. $^{12}C_2H_6$ diffusion was much faster than that of $^{13}C_2H_6$ in the heating phase, resulting in $\delta^{13}C_2$ becoming lighter. Besides, the adsorbability of $^{13}CH_4$ and $^{13}C_2H_6$ was stronger than those of $^{12}CH_4$ and $^{12}C_2H_6$, respectively, leading to $^{13}CH_4$ and $^{13}C_2H_6$ enrichment in Phases II and III.

Previous studies had reported that the shale gases from the Lower Paleozoic strata in West Hubei had a positive relationship with the carbon isotope fractionation degree of CH_4.[20] Also, the given shale intervals from LCNF of the middle Yangtze region were characteristic of high shale gas content, accompanied by isotopic fractionation of CH_4 of the corresponding mud gases and cutting-released gases.[9] Figure 12a shows that the desorbed gas content correlated weakly with carbon isotope fractionation. This occurrence could be attributed to the difference in the desorption time of the last desorbed samples of each core sample, which varies inherently and considerably. Such as the SZY1−1 sample with the shortest desorbed time of the last desorbed samples of 20.94 h and the SZY1−9 sample with the longest desorbed time of the last desorbed samples of 59.43 h. Thus, the value of $\delta^{13}C_1$ in the desorbed samples with 21 h desorption time ($\delta^{13}C_{1L21}$) replaces those of the last desorbed samples in the cross plots (Figure 12b). The correlation between the desorbed gas content and the carbon isotope fractionation degree ($\Delta\delta^{13}C_{1L21\text{-}F}$) of all nine core samples improved (Figure 12b).

Additionally, the TOC correlated positively with the carbon isotope fractionation degree ($\Delta\delta^{13}C_{1L21\text{-}F}$) (Figure 12c). The higher the TOC of the shales, the more the micropores/nanopores, and the better the adsorption capability.[33] Due to the stronger adsorption capability of $^{13}CH_4$ relative to $^{12}CH_4$, more substantial carbon isotope fractionation ensued.

Summarily, the carbon isotope fractionation of desorbed CH_4 and C_2H_6 from the nine shale core samples (from the LCNF of the SZY1 well) occurred via adsorption/desorption and diffusion. $^{12}C_2H_6$ diffusion was temperature-sensitive, and its diffusion rate was much faster than that of $^{13}C_2H_6$ in the heating phase. Therefore, the temperature could be an external factor in reducing the carbon isotope fractionation of a specific gas at a particular desorption phase. In contrast, pressure is the other external factor facilitating carbon isotope fractionation.[34] This condition was why CH_4 was isotopically heavier during production, owing to a lowering of pressure after the hydraulic fracturing.

Furthermore, the degree of carbon isotope fractionation should be used, provided that the desorption time of the last desorbed samples is equal or similar for all shale core samples. The carbon isotope fractionation degree is a viable indicator of sweet spots for shale gas exploration and production. Figure 12d suggests that the desorbed gas contents of the shale core samples correlated positively with the $\delta^{13}C_1$ of the last desorbed gas samples ($\delta^{13}C_{1L21}$). Such a result indicates that $\Delta\delta^{13}C_{1L21\text{-}F}$ is a contemporary indicator for the desorbed gas contents.

3.5. Genetic Source of the Shale Gas. Geochemical characterization (such as chemical composition analysis and stable carbon isotopy) of gases is commonly used to identify

https://doi.org/10.1021/acsomega.3c08330
ACS Omega 2024, 9, 13764−13781

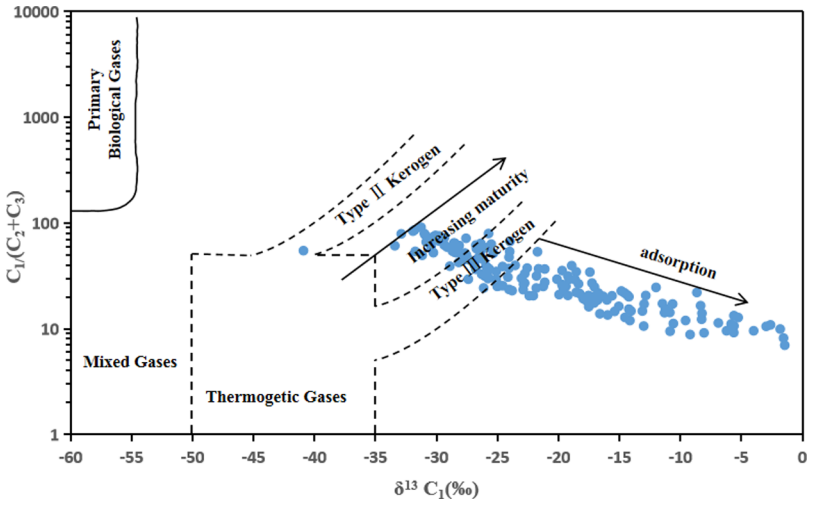

Figure 13. Diagram of $\delta^{13}C_1$ versus $C_1/(C_2 + C_3)$ of desorbed shale gas samples to determine the genetic source of Lower Cambrian shale gas in MTZSS (Adapted with permission from Whiticar, 1999, Elsevier B.V.).

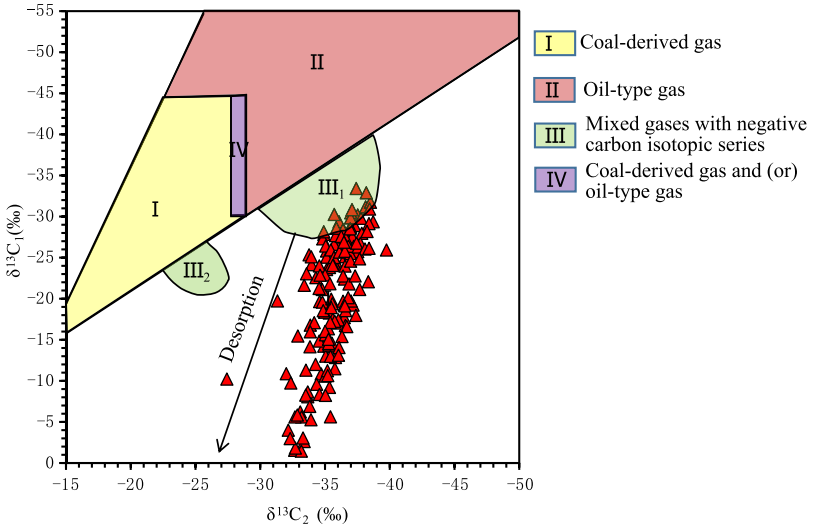

Figure 14. Diagram of $\delta^{13}C_1$ versus $\delta^{13}C_2$ of the desorbed shale gas samples to determine the genetic source of Lower Cambrian shale gas in MTZSS (Adapted with permission from Dai et al., 2014, Elsevier B.V.). The lower Cambrian Niutitang shale gases in MTZSS belong to mixed gases with negative carbon isotopic series, and the desorption caused the distribution of outside Region III_1 for most desorbed gas samples.

the origins of natural gases,[7−9,19,75,77] their evolution, migration, and accumulation.[78] Shale gas preserves the original geochemical characteristics in a sealed system because of the gas' self-generation and self-storage. Thus, the migration distance is much shorter than or even negligible. Therefore, the migration and geochemical characteristics can be ignored compared to generation, evolution, and accumulation occurring in the closed system of the shale itself before desorption. Nevertheless, the adsorbability of the shale to both hydrocarbon components and isotopologues differs significantly, causing the compositional and isotopic fractionation of shale gas. Therefore, the fractionation effects must be considered when using these parameters for the genetic source identification of shale gases.

According to the diagram of $\delta^{13}C_1$ versus $C_1/(C_2 + C_3)$,[79] the desorbed gases were distributed outside the region of thermogenic gases (Figure 13). However, with maturity, $C_1/(C_2 + C_3)$ and $\delta^{13}C_1$ were thermally increased during the high maturation,[8,20,80,81] while the desorption leads to the considerable carbon isotope fractionation.[20,34,38,74] The R_o of the shale core samples of SZY1 Well informed us that these shales were within the high-over mature range (Table 1). Thus, all desorbed gases were thermogenic when high maturity and isotope fractionation effects were considered (Figure 13).

Because $\delta^{13}C_2$ retains the original genetic information on gases, its value is one of the most frequently used indicators to determine the genetic source of gases.[19,20,82,83] In general, the $\delta^{13}C_2$ value of oil-type gas is ←29‰, whereas that of coal-formed gas is >−28‰.[82] These gases, derived from various precursors, increased with maturity. The majority of the $\delta^{13}C_2$ values of all desorbed samples were ←29‰ (Table 1, Figure 14), suggesting that the shale gases from LCNF in MTZSS belong to the oil-type gas.

The oil-type gas originates from the thermal cracking of kerogen and oil, which are widely distributed in nature and difficult to differentiate. Hence, a genetic diagram of $\ln(C_1/C_2)$ versus $\ln(C_2/C_3)$ was employed to distinguish oil-cracking gas from kerogen-cracking gas.[20,42,70,84,85] The principle is that the kerogen-cracking gas originates from the demethylation of kerogen. CH_4 is the main component of demethylated

https://doi.org/10.1021/acsomega.3c08330
ACS Omega 2024, 9, 13764−13781

products, substantially characterized by the rapid increase in the CH_4 content versus the slow generation of C_2H_6 and C_3H_8. Thus, C_1/C_2 increases rapidly, whereas C_2/C_3 increases slowly or almost unchanged.

Oil-cracking gas refers to the secondary cracking of oil. It is derived from the carbon−carbon cleavage of long aliphatic oil chains, resulting in large quantities of C_2H_6 and C_3H_8. Accordingly, the C_2/C_3 ratio varies more comprehensively than the unchanged C_1/C_2 ratio. Figure 15 shows that all

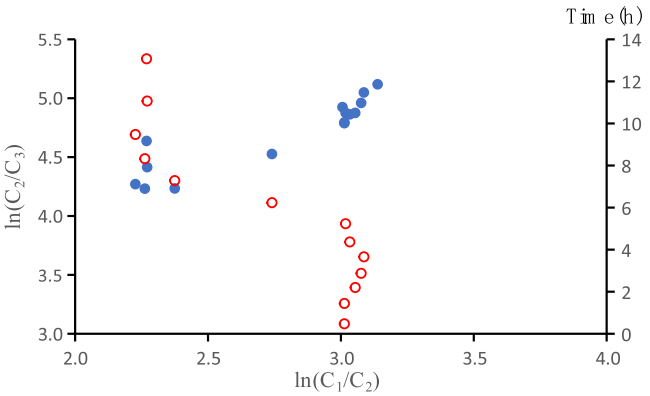

Figure 15. Crossplots of $\ln(C_1/C_2)$ versus $\ln(C_2/C_3)$ (blue solid dot) and desorbed time (red hollow dot).

desorbed gas samples' C_1/C_2 ratios had an overall downward trend, although the values were stable in each temperature phase. Furthermore, regarding the SZY1−3 sample, one of the two shale core samples contained propane. The C_1/C_2 ratios of the desorbed samples varied in a narrower range compared to C_2/C_3 ratios at the beginning of the desorption (Figure 15). These observations suggest that the shale gases from LCNF in MTZSS are predominantly oil-cracking gases, and the absence of propane is due to the highly/overmature shales. Such observation coincides with the view that the shale of type I kerogen is considered a good gas source because all oils cracked to wet gas when R_o is >1.4%. In comparison, all condensate-rich gases cracked to dry gas when R_o is >2.0%[56] due to the primary type I organic matter of LCNF shales in MTZSS. Nevertheless, the gas generation from type I kerogen cracking at low and high maturity is inevitable.[42] $\delta^{13}C_1$ versus $\delta^{13}C_2$ diagram proposed by Dai et al. (2014) pointed out that the Niutitang shale gas of the study area belongs to mixed gas (Figure 14). Consequently, the shale gases from LCNF in MTZSS are primarily composed of oil-cracking gases mixed with kerogen-cracking gases. This observation is consistent with those in the Lower Cambrian Qiongzhusi (Niutitang) shale in the Weiyuan Block of Sichuan Basin in the Upper Yangtze region and the LCNF shale in the Yichang Block of west Hubei in the Middle Yangtze region.[85]

3.6. Feature and Origin of Carbon Isotope Reversal.

Based on carbon isotope thermodynamic fractionation, the carbon isotopic differentiation of the natural gas components is a widespread phenomenon during gas exploration and production.[8,9,19,20,39−41] Specifically, all the LCNF shale gases in highly over-mature shales in China are characteristic of CIR.[5−9] Similarly, LCNF shale gas in the Yichang Block of west Hubei of Middle Yangtze region[6,8,9] and Lower Cambrian Qiongzhusi (Niutitang) shale gas in the southeast and northeast Sichuan Basin of Upper Yangtze region[5,7] exhibit similar property. This phenomenon is mainly caused by the secondary cracking of oils, which is accompanied by the cracking of kerogen. Previous researchers have observed a usual isotopic trend in the Lower Cambrian Qiongzhusi shale gas of Xiushan of southeast Chongqing.[23] However, the gases used in this study were residual gas extracted by vacuum crushing from the outcrop shale samples of the Qiongzhusi Formation. In the early stages of diagenesis, the remaining gas is reserved in the pores generated by diagenesis. These pores are sealed in the later stage of diagenesis (and even Catagensis), resulting in disconnected pores. Thus, the gas could not be desorbed. Therefore, the remaining gases belong to Region III for the trend of maturity-dependent $\delta^{13}C_2$ and $\delta^{13}C_1$ variation.[86]

The carbon isotopic composition of CH_4 and C_2H_6 of all desorbed shale gas samples of Lower Cambrian in south Shanxi is characterized by a reversed sequence of carbon isotope ($\delta^{13}C_1 > \delta^{13}C_2$) (Figures 16a,b). The degree of CIR of the last desorbed gas samples is much larger than that of the first desorbed gas samples (Figure 16a,b), caused by more significant carbon isotope fractionation of $\delta^{13}C_1$ than of $\delta^{13}C_2$. The higher the shale maturity, the higher the wetness and the lighter the $\delta^{13}C$ of the secondary cracking gas, caused by conversion (between oil and condensate) and carbon−carbon cleavage. The proportion of the second cracking gas in the mixed gases gradually increases during maturation, whereas the percentage of C_{2+} is relatively high and thus gives rise to $^{12}C_2$ enrichment. When a specific level of maturity is reached, and $^{12}C_2$ carbon is enriched to a degree, CIR will occur.[43] Based on this theory, a previous study proposed dividing the CIR into four regions.[86] The gas samples in this study belonged to Region III of the diagram based on the maturity-dependent $\delta^{13}C_2$ and $\delta^{13}C_1$ trends during maturation (Figure 17).

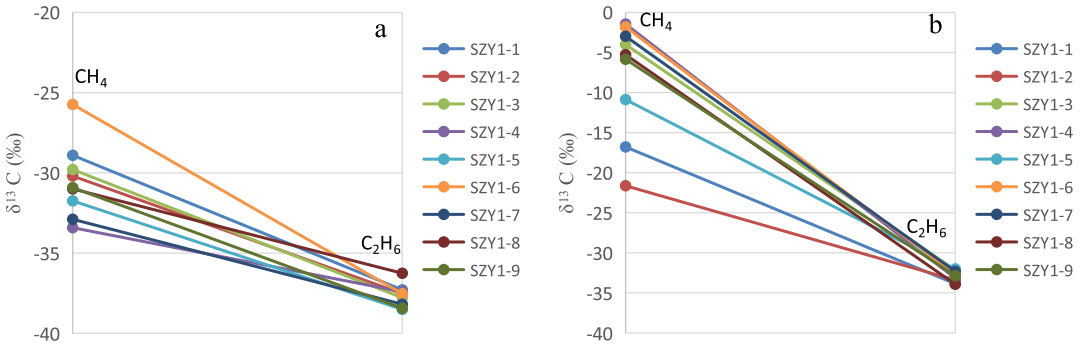

Figure 16. Degree of carbon isotope reversal of the first desorbed gas samples (a) and the last desorbed gas samples (b).

https://doi.org/10.1021/acsomega.3c08330
ACS Omega 2024, 9, 13764−13781

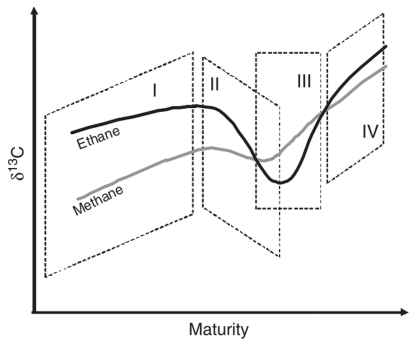

Figure 17. A complete trend of maturity-dependent $\delta^{13}C_2$ and $\delta^{13}C_1$ variation.[86] Regions: I—normal trend; II—$\delta^{13}C_2$ reversal with respect to maturity trend; III—$\delta^{13}C$ reversal against carbon number ($\delta^{13}C_1 > \delta^{13}C_2$); IV—normal trend (Adapted with permission from Xia et al., 2013, Elsevier B.V.).

The CIR of CH_4 and C_2H_6 of all desorbed shale gas samples of LCNF in MTZSS arose mainly from cracking residual soluble organic matter (oil, condensate, and asphaltene) at the high-overmature stage, coupled with the cracking of kerogen at the early maturation stage. Such an observation agrees with the explanation from the diagram of $\delta^{13}C_1$ versus $\delta^{13}C_2$ of the desorbed shale gas samples (Figure 14). In addition, even though the diffusion of shale gas is minimal because shale gas is an unconventional natural gas, the shale strata have been raised over a long geological period, causing CIR diffusion.[20,87]

According to the burial and thermal history of adjacent wells in south Shanxi, the lower Cambrian shales were raised significantly, owing to the two Yanshanian and Himalayan tectonic movements.[13] Therefore, diffusion is an indispensable factor in the LCNF shale gas's CIR in MTZSS since CIR is the cumulative result of many factors. Furthermore, Figure 18

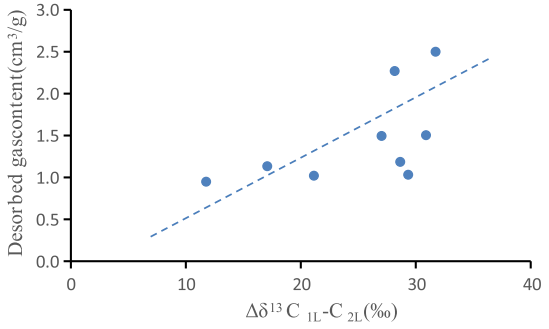

Figure 18. Crossplots of desorbed shale gas content versus the degree of carbon isotope reversal of the last desorbed gas samples ($\Delta\delta^{13}C_{1L}-C_{2L}$).

shows that the degree of CIR of the last desorbed samples correlated positively with the desorbed gas content. As an inference, the degree of CIR could be a valuable indicator to determine sweet spots of shale gas in south Shanxi.

3.7. Indicators for Identifying Shale Gas Sweet Spots for the Exploration and Production. The desorbed gas content is inversely proportional to the dryness index of the last desorbed gas samples of each core sample (Figure 9a) while the desorbed gas content did not correlate with the dryness index of the first desorbed gas of each core sample (Figure 9b). Namely, the desorbed gas content increases with the decrease of dryness index at the end of desorption, which coincided well with many reports[20,66,67] and is thought to be a result of various adsorbability of the shale to gaseous hydrocarbon. Consequently, the dryness index of the last desorbed gas of the core sample is a useful indicator of sweet spots for shale gas exploration and production.

The calculation of the carbon isotope fractionation degree should follow a rule that the desorbed time of the last desorbed samples must be the same or very close for all shale core samples. Based on this rule, the desorbed gas contents of shale core samples correlated positively with the carbon isotope fractionation degree ($\Delta\delta^{13}C_{1L21\text{-}f}$) (Figures 12b), and the carbon isotope fractionation degree ($\Delta\delta^{13}C_{1L21\text{-}f}$) is an effective indicator of sweet spots for shale gas exploration and production. Besides, Figure 12d suggests that the desorbed gas contents of shale core samples had a positive relation with the $\delta^{13}C_1$ of the last desorbed gas samples ($\delta^{13}C_{1L21}$), suggesting that it is also the same indicator of sweet spots for shale gas exploration and production as $\Delta\delta^{13}C_{1L21\text{-}f}$

The carbon isotope reversal (CIR) ($\delta^{13}CH_4 > \delta^{13}C_2H_6$) of the natural gas components is a common phenomenon during gas exploration and production.[8,9,19,20,39−41] Specifically, all the LCNF shale gases in highly over-mature shales in China are characteristic of CIR,[5−9] also which is caused by the cracking of the residual soluble organic matter at the high overmaturity stage mixed with the cracking of kerogen at the early stage of maturation as well as the diffusion of gas. Figure 18 exhibits that the degree of CIR of the last desorbed samples is positively related to the desorbed gas content, deciphering the degree of CIR ($\Delta\delta^{13}C_{1L}-C_{2L}$) could be a useful indicator to determine sweet spots of shale gas.

In a word, the last desorbed shale gas samples featured by a low value of the dryness index, high values of $\delta^{13}C_1$, high carbon isotope fractionation, and a CIR degree indicate shale gas sweet spots for the exploration and production of LCNF in MTZSS, which probably can be applied to LCNF shale gas in the other exploration blocks of South China.

4. CONCLUSIONS

Based on scientific analyses, the LCNF shale in south Shanxi was more of a gas-rich and high gas interval, indicating the excellent shale gas resource potential of the LCNF of MTZSS.

The desorbed gases were composed of plenty of hydrocarbon gases (predominantly CH_4) and a small amount of nonhydrocarbon gases. The former consisted of CH_4, C_2H_6, and a minute amount of C_3H_8 found only in the SZY1−3 and SZY1−4 core samples. The nonhydrocarbon gases were H_2, CO_2, and a minute quantity of He found in the SZY1−2 core sample. Overall, the gas components increased during desorption, except for CH_4 and He. Based on the ratio between the two gases, with an increase in desorption time and temperature, the sequence of adsorbability of the shale for different gases was $H_2 > CO_2 > C_2H_6 > CH_4 > He$.

The value of $\delta^{13}C_1$ of the desorbed samples gradually became heavier until the desorption experiments were over. The $\delta^{13}C_2$ value had the same changing trend as CH_4, but it frequently fluctuated due to the increasing temperature.

Also, the shorter the exposure time of core shale, the lighter the $\delta^{13}C$ at the beginning of desorption, which is ascribed to the preferential release of $\delta^{13}C$ during desorption. The carbon isotope fractionation of the desorbed CH_4 and C_2H_6 of nine gas-bearing shale core samples from the LCNF of the SZY1 well was determined jointly by adsorption/desorption and diffusion.

https://doi.org/10.1021/acsomega.3c08330
ACS Omega 2024, 9, 13764−13781

Through the analytical diagrams of $\ln(C_1/C_2)$ versus $\ln(C_2/C_3)$, $\delta^{13}C_1$ versus $C_1/(C_2 + C_3)$, and $\delta^{13}C_1$ versus $\delta^{13}C_2$, the shale gases from LCNF of south Shanxi primarily consist of oil-cracking gases mixed with kerogen-cracking gases, which is the dominant cause of CIR. Additionally, diffusion is an indispensable factor in CIR since the lower Cambrian shales in MTZSS experienced significant uplift due to the Yanshanian and Himalayan tectonic movements.

Furthermore, the desorbed gas content had positive and negative relationships with the corresponding isotopic reversal degree and gas dryness index of the last desorbed samples, respectively. The degree of CH_4 carbon isotope fractionation and $\delta^{13}C_1$ of the last desorbed gas samples correlated positively to the desorbed gas content. Thus, calculating carbon isotope fractionation degree could be used when the desorption time of the last desorbed samples is the same or similar for all shale core samples. Hence, the four parameters can be effective indicators for identifying shale gas sweet spots for the exploration and production of LCNF in MTZSS.

AUTHOR INFORMATION

Corresponding Authors

Bin Shen − *National Research Center for Geoanalysis, Chinese Academy of Geological Science, Beijing 100037, China;* orcid.org/0009-0003-2904-3805; Email: shenbin1007@163.com

Tao Tian − *Shaanxi Coal Geology Group Co., Ltd. Key Laboratory of Coal Resources Exploration and Comprehensive Utilization, Ministry of Natural Resources, Xi'an 710021, China*; Email: tiantao870211@163.com

Authors

Xiaotao Zhang − *National Research Center for Geoanalysis, Chinese Academy of Geological Science, Beijing 100037, China;* orcid.org/0000-0001-9925-9378

Shizhen Li − *Oil and Gas Survey, China Geological Survey, Beijing 100083, China;* orcid.org/0000-0002-3681-0449

Xuemin Xu − *National Research Center for Geoanalysis, Chinese Academy of Geological Science, Beijing 100037, China;* orcid.org/0000-0001-7107-9180

Jiajia Yang − *National Research Center for Geoanalysis, Chinese Academy of Geological Science, Beijing 100037, China*

Weilin Sun − *National Research Center for Geoanalysis, Chinese Academy of Geological Science, Beijing 100037, China*

Jing Qin − *National Research Center for Geoanalysis, Chinese Academy of Geological Science, Beijing 100037, China*

Complete contact information is available at: https://pubs.acs.org/10.1021/acsomega.3c08330

Notes

The authors declare no competing financial interest.

ACKNOWLEDGMENTS

This study was supported by Key Parameter Testing for Shale Gas in Key Areas of Southern China (DD20230265) of China Geological Survey, Shaanxi Province 2023 Innovation Capability Support Plan (2023KJXX-122), National Natural Science Foundation of China (Grants No. 41702159), and Rock macerals in situ SEM analysis and three-dimensional interspace reconstruction technology (CSJ-2023-09). We appreciate Shaanxi Coal Geological Oil and gas Drilling Co., Ltd. for all the help in collecting gas and core samples. Besides, we are grateful to the editors and all reviewers for their valuable suggestions that we have used to improve the quality of our manuscript.

REFERENCES

(1) Price, L. C.; Schoell, M. Constraints on the origins of hydrocarbon gas from compositions of gases at their site of origin. *Nature* **1995**, *378*, 368−371.

(2) Zou, C. N.; Yang, Z.; Pan, S. Q.; Chen, Y. Y.; Lin, S. H.; Huang, J. L.; Wu, S. T.; Dong, D. Z.; Wang, S. F.; Liang, F.; Sun, S. S.; Huang, Y.; Weng, D. W. Shale gas formation and occurrence in China: an overview of the current status and future potential. *Acta Geol. Sin.* **2016**, *90* (4), 1249−1283.

(3) Jin, Z. J.; Nie, H. K.; Liu, Q. Y.; Zhao, J. H.; Jiang, T. Source and seal coupling mechanism for shale gas enrichment in upper ordovician Wufeng Formation - lower silurian Longmaxi Formation in Sichuan Basin and its periphery. *Mar. Petrol. Geol.* **2018**, *97*, 78−93.

(4) Zhai, G. Y.; Wang, Y. F.; Zhou, Z.; Liu, G. H.; Yang, Y. R.; Li, J. "Source-diagenesis-accumulation" enrichment and accumulation regularity of marine shale gas in southern china. *China Geol. (English Edition)* **2018**, *1* (3), 319−330.

(5) (In Chinese with English Abstract) Han, H.; Li, D. H.; Ma, Y.; Cheng, L. J.; Wang, Q.; Zhong, N. N. The origin of marine shale gas in the northeastern sichuan basin, china: implications from chemical composition and stable carbon isotope of desorbed gas. *Acta Petrol. Sin.* **2013**, *34* (3), 453−459.

(6) Liu, Y.; Zhang, J. C.; Ren, J.; Liu, Z. Y.; Huang, H.; Tang, X. Stable isotope geochemistry of the nitrogen-rich gas from lower cambrian shale in the yangtze gorges area, south china. *Mar. Pet. Geol.* **2016**, *77*, 693−702.

(7) Zhang, S. C.; He, K.; Hu, G. Y.; Mi, J. K.; Ma, Q. S.; Liu, K. Y.; Tang, Y. C. Unique chemical and isotopic characteristics and origins of natural gases in the paleozoic marine formations in the sichuan basin, sw china: isotope fractionation of deep and high mature carbonate reservoir gases. *Mar. Pet. Geol.* **2018**, *89*, 68−82.

(8) (in Chinese with English abstract) Luo, S. Y.; Chen, X. H.; Liu, A.; Li, H.; Sun, C. Characteristics and geological significance of canister desorption gas from the Lower Cambrian Shuijingtuo Formation shale in Yichang area, Middle Yangtze Region. *Acta Pet. Sin.* **2019**, *40* (8), 941−955.

(9) (in Chinese with English abstract) Zhang, J. Z.; Zhu, D.; Ci, X. H.; Niu, Q.; Zhang, H. X.; Tang, Y. C.; Kang, S. J.; He, K. Characteristics of carbon isotope while drilling and exploration significance of shale gas in Niutitang and Doushantuo formations in Well Eyangye-2, Yichang, Hubei, China. *Acta Pet. Sin.* **2019**, *40* (11), 1346−1357.

(10) (in Chinese with English abstract) Xu, T.; Xu, F.; Guo, Y. H.; Wang, N.; Xie, Q.; Huang, W. Organic geochemical characteistics of the lower paleozoic shales in xixiang-zhenba area, southern shaanxi. *J. Northeast Petrol. Univ.* **2019**, *43* (4), 59−68.

(11) (in Chinese with English abstract) Wang, P. F.; Jiang, Z. X.; Yang, C. H.; Jing, C.; Lv, P.; Wang, H. H. Organic pore development characteristics of Longmaxi and Niutitang shales in the periphery of Chongqing. *Lithol. Reservoirs* **2019**, *31* (3), 27−36.

(12) Chen, X.; Zhai, G.; Bao, S.; Pang, F.; Wang, J.; Tong, C. Shale gas accumulation and gas-bearing properties of niutitang formation in well zhendi 1,zhenba region of southern shaanxi province, China. *Min. Mag.* **2018**, *27* (S1), 101−106.

(13) Tian, T.; Yang, P.; Ren, Z. L.; Fu, D. L.; Li, J. Hydrocarbon migration and accumulation in the lower cambrian to neoproterozoic reservoirs in the micangshan tectonic zone, china: new evidence of fluid inclusions. *Energy Rep.* **2020b**, *6*, 721−733.

(14) Liu, Z. X.; Yan, D. T.; Du, X. B.; Li, S. J. Organic matter accumulation of the early Cambrian black shales on the flank of Micangshan-Hannan Uplift, northern upper Yangtze Block. *South China. J. Petrol. Sci. Eng.* **2021**, *200*, No. 108378.

https://doi.org/10.1021/acsomega.3c08330
ACS Omega 2024, 9, 13764−13781

(15) Gensterblum, Y.; Busch, A.; Krooss, B. M. Molecular concept and experimental evidence of competitive adsorption of H_2O, CO_2 and CH_4 on organic material. *Fuel* **2014**, *115*, 581−588.
(16) Martini, A. M.; Walter, L. M.; Budai, J. M.; et al. Genetic and temporal relations between formation waters and biogenic methane: upper Devonian Antrim Shale, Michigan Basin, USA. *Geochem. Cosmochim. Acta* **1998**, *62* (10), 1699−1720.
(17) Curtis, J. B. Fractured shale-gas systems. *AAPG Bull.* **2002**, *86* (11), 1921−1938.
(18) Mengal, S. A., Wattenbarger, R. A. Accounting for adsorbed gas in shale gas reservoirs. In: *SPE Middle East Oil and Gas Show and Conference*; SPE, 2011.
(19) Dai, J. X.; Zou, C. N.; Liao, S. M.; Dong, D. Z.; Ni, Y. Y.; Huang, J. L.; Wu, W.; Gong, D. Y.; Huang, S. P.; Hu, G. Y. Geochemistry of the extremely high thermal maturity Longmaxi shale gas, southern Sichuan Basin. *Org. Geochem.* **2014**, *74*, 3−12.
(20) Li, S. Z.; Meng, F. Y.; Zhang, X. T.; Zhou, Z.; Shen, B.; Wei, S. Y.; Zhang, S. S. Gas composition and carbon isotopic variation during shale gas desorption: implication from the ordovician wufeng formation - silurian longmaxi formation in west hubei, china. *J. Nat. Gas Sci. Eng.* **2021**, *87* (4), 103777.
(21) Javadpour, F.; Fisher, D.; Unsworth, M. Nanoscale gas flow in shale gas sediments. *J. Can. Pet. Technol.* **2007**, *46* (10), No. PETSOC-07-10-06.
(22) Yang, T. Y.; Li, X.; Zhang, D. X. Quantitative dynamic analysis of gas desorption contribution to production in shale gas reservoirs. *J. Unconv. Oil Gas Resour.* **2015**, *9*, 18−30.
(23) Xu, H.; Zhou, W.; Cao, Q.; Xiao, C.; Zhou, Q. M.; Zhang, H. T.; Zhang, Y. Y. Differential fluid migration behaviour and tectonic movement in lower silurian and lower cambrian shale gas systems in china using isotope geochemistry. *Mar. Pet. Geol.* **2018**, *89*, 47−57.
(24) Kalkreuth, W.; Holz, M.; Casagrande, J.; Cruz, R.; Oliveira, T.; Kern, M.; Levandowski, J.; Rolim, S. The Coalbed Methane (CBM) potential of the Santa Terezinha coalfield − 3D modeling and evaluation of exploration well CBM001-ST-RS. *Rev. Bras. Geociencias* **2008**, *38* (2), 3−17.
(25) Ma, Y.; Zhong, N. N.; Yao, L. P.; Huang, H. P.; Larter, S.; Jiao, W. W. Shale gas desorption behavior and carbon isotopic variations of gases from canister desorption of two sets of gas shales in south china. *Mar. Pet. Geol.* **2020**, *113*, 104127.
(26) Schoell, M. Genetic characterization of natural gases. *AAPG Bull.* **1983**, *67*, 2225−2238.
(27) Scott, A.; Kaiser, W.; Ayers, W. Thermogenic and secondary Biogenic gases, san juan basin, colorado and New Mexico−implications for coalbed gas producibility. *AAPG Bull.* **1994**, *78*, 1186−1209.
(28) Whiticar, M. J. Carbon and hydrogen isotope systematics of bacterial formation and oxidation of methane. *Chem. Geol.* **1999**, *161*, 291−314.
(29) Galimov, E. M. Isotope organic geochemistry. *Org. Geochem.* **2006**, *37*, 1200−1262.
(30) Golding, S. D.; Boreham, C. J.; Esterle, J. S. Stable isotope geochemistry of coal bed and shale gas and related production waters: a review. *Int. J. Coal Geol.* **2013**, *120*, 24−40.
(31) Zhang, T. W.; Krooss, B. M. Experimental investigation on the carbon isotope fractionation of methane during gas migration by diffusion through sedimentary rocks at elevated temperature and pressure. *Geochem. Cosmochim. Acta* **2001**, *65*, 2723−2742.
(32) (in Chinese with English abstract) Duan, L. J.; Tang, S. H.; Liu, H. L.; Zhu, B. C. The impact of coal reservoir physical properties on carbon isotope fractionation of coalbed methane. *Acta Geol. Sin.* **2008**, *82* (10), 1330−1334.
(33) Milliken, K. L.; Rudnicki, M.; Awwiller, D. N.; Zhang, T. W. Organic matter−hosted pore system, marcellus formation (devonian), pennsylvania. *AAPG Bull.* **2013**, *97* (2), 177−200.
(34) Wei, Y. B.; Lu, S. F.; Li, J. Q.; Yu, R. Z.; Li, W. B.; Cheng, F.; Fu, C. B.; Zhao, T. L.; Feng, W. J.; Song, Z. J. Impacts of gas pressure on carbon isotope fractionation during methane degassing—an experimental study on shales from wufeng and longmaxi formations in southeast sichuan, china. *Mar. Pet. Geol.* **2021**, *128*, No. 105001.
(35) Schloemer, S.; Krooss, B. M. Molecular transport of methane, ethane and nitrogen and the influence of diffusion on the chemical and isotopic composition of natural gas accumulations. *Geofluids* **2010**, *4* (1), 81−108.
(36) Xia, X. Y.; Tang, Y. C. Isotope fractionation of methane during natural gas flow with coupled diffusion and adsorption/desorption. *Geochem. Cosmochim. Acta* **2012**, *77*, 489−503.
(37) Harpalani, S.; Chen, G. Influence of gas production induced volumetric strain on permeability of coal. *Geotech. Geol. Eng.* **1997**, *15* (4), 303−325.
(38) Liu, P.; Wang, X.; Lin, Y.; Liu, C.; Li, X.; Liu, W. Chemical and carbon isotope fractionations of alkane gases desorbed from confined systems and the application toward shale gas reservoir. *Mar. Petrol. Geol.* **2020**, *113*, No. 104103.
(39) Zumberge, J.; Ferworn, K.; Brown, S. Isotopic reversal('roll-over') in shale gases produced from the Mississippian Barnett and Fayetteville formations. *Mar. Petrol. Geol.* **2012**, *31* (1), 43−52.
(40) Xia, X. Y.; Chen, J.; Braun, R.; Tang, Y. C. Isotopic reversals with respect to maturity trends due to mixing of primary and secondary products in source rocks. *Chem. Geol.* **2013**, *339* (2), 205−212.
(41) Tilley, B.; Muehlenbachs, K. Isotope reversals and universal stages and trends of gas maturation in sealed, self-contained petroleum systems. *Chem. Geol.* **2013**, *339*, 194−204.
(42) Hao, F.; Zou, H. Y. Cause of shale gas geochemical anomalies and mechanisms for gas enrichment and depletion in high-maturity shales. *Mar. Petrol. Geol.* **2013**, *44* (3), 1−12.
(43) Tang, Y. C.; Perry, J. K.; Jenden, P. D.; Schoell, M. Mathematical modeling of stable carbon isotope ratios in natural gases. *Geochem. Cosmochim. Acta* **2000**, *64* (15), 2673−2687.
(44) Burruss, R. C.; Laughrey, C. D. Carbon and hydrogen isotopic reversals in deep basin gas: evidence for limits to the stability of hydrocarbons. *Org. Geochem.* **2010**, *41* (12), 1285−1296.
(45) Prinzhofer, A.; Pernaton, R. Isotopically light methane in natural gas: bacterial imprint or diffusive fractionation. *Chem. Geol.* **1997**, *142* (3−4), 193−200.
(46) Tilley, B.; Mclellan, S.; Hiebert, S.; Quartero, B.; Veilleux, B.; Muehlenbachs, K. Gas isotope reversals in fractured gas reservoirs of the western canadian foothills: mature shale gases in disguise. *AAPG Bull.* **2011**, *95* (8), 1399−1422.
(47) (in Chinese with English abstract) Tian, T.; Zhou, S. X.; Fu, D. L.; Yang, F.; Duan, Z. H.; Li, J. Composition of carbon isotope of Niutitang Formation in Micangshan-Hannan Uplift and its significances. *J. China Univ. Petrol.* **2019a**, *43* (4), 40−51.
(48) (in Chinese with English abstract) Tian, T.; Fu, D. L.; Zhou, S. X.; Yang, F.; Li, J. The paleo-redox conditions of the shale in Niutitang Formation and its effects on organic matter enrichment of the Micangshan-Hannan Uplift. *J. Lanzhou Univ. Nat. Sci.* **2020a**, *56* (1), 37−47.
(49) (in Chinese with English abstract) Chen, X. L.; Zhai, G. Y.; Bao, S. J.; Pang, F.; Wang, J. Z.; Tong, C. C. Shale gas accumulation and gas-bearing properties of Niutitang formation in well Zhendi 1, Zhenba region of southern Shaanxi province, China. *Min. Mag.* **2018**, *27* (S1), 101−106.
(50) Tian, T.; Zhou, S. X.; Fu, D.; Yang, F.; Li, J. Calculation of the original abundance of organic matter at high-over maturity: a case study of the LCNF shale in the micangshan-hannan uplift, sw china. *J. Petrol. Sci. Eng.* **2019**, *179*, 645−654.
(51) (in Chinese with English abstract) Tian, T.; Fu, D. L.; Yang, F.; Duan, Z. H.; Lin, Y. B.; Zhao, X. J. Relationship between mineral composition and micro-pores of Niutitang-Formation shale in Micangshan-Hannan Uplift. *J. China Coal Soc.* **2018**, *43* (S1), 236−244.
(52) (in Chinese with English abstract) Li, H. B.; Wang, Z.; Xu, F.; Jin, K.; Wang, N. Shale gas reservoirs characteristics of Micang Mountain uplift in the north of the Sichuan Basin. *Unconv. Oil Gas* **2019**, *6* (6), 1−6.

https://doi.org/10.1021/acsomega.3c08330
ACS Omega 2024, 9, 13764−13781

(53) (in Chinese with English abstract) Pei, X. Z.; Li, R. B.; Ding, S. P.; Liu, Z. Q.; Li, Z. C.; Feng, J. Y.; Sun, Y.; Zhang, Y. F. Tectonic intersection relationship between dabashan and micangshan in zhenba area,southern shaanxi province. *Oil Gas Geol.* **2009**, *30* (5), 576−583.
(54) (in Chinese with English abstract) Xu, H. M.; Liu, S.; Qu, G. S.; Li, Y. F.; Sun, G.; Liu, K. Structural characteristics and formation mechanism in the Micangshan Foreland. *South China. Acta Geol. Sin.* **2009**, *83* (1), 81−91.
(55) Zhang, X. T.; Shen, B.; Yang, J. J.; Sun, W. L.; Hou, D. J. Evolution characteristics of maturity-related sterane and terpane biomarker parameters during hydrothermal experiments in a semi-open system under geological constraint. *J. Petrol. Sci. Eng.* **2021**, *201*, 108412.
(56) Qin, J.; Wang, S. Q.; Sanei, H.; Jiang, C. Q.; Chen, Z. H.; Ren, S. M.; Xu, X.; Yang, J.; Zhong, N. Revelation of organic matter sources and sedimentary environment characteristics for shale gas formation by petrographic analysis of middle jurassic dameigou formation, northern qaidam basin, china. *Int. J. Coal Geol.* **2018**, *195*, 373−385.
(57) (in Chinese with English abstract) Feng, G. X.; Chen, S. J. Relationship between the reflectance of bitumen and vitrinite in rock. *Nat. Gas Ind.* **1988**, *3*, 30−35.
(58) (in Chinese with English abstract) Burnaman, M. D.; Xia, W. W.; Shelton, J. Shale gas play screening and evaluation criteria. *China Petrol. Exp.* **2009**, *14*, 51−64.
(59) Topor, T.; Derkowski, A.; Ziemianski, P.; Szczurowski, J.; McCarty, D. K. The effect of organic matter maturation and porosity evolution on methane storage potential in the Baltic Basin (Poland) shale-gas reservoir. *Int. J. Coal Geol.* **2017**, *180*, 46−56.
(60) Tinni, A., Sondergeld, C. H., Rai, C. S. Hydrocarbon storage mechanism in shale reservoirs and impact on hydrocarbon production. In *Unconventional Resources Technology Conference*; Austin, Texas, USA, 2017.
(61) Brunauer, S.; Deming, L. S.; Deming, W. S.; Teller, E. On a theory of Van der Waals adsorption of gases. *J. Am. Chem. Soc.* **1940**, *62*, 1723−1732.
(62) Choi, J.; Do, D. D.; Do, H. D. Surface diffusion of adsorbed molecules in porous media: monolayer, multilayer, and capillary condensation regimes. *Ind. Eng. Chem. Res.* **2001**, *40*, 4005−4031.
(63) Cao, Z.; Jiang, H.; Zeng, J. H.; Saibi, H.; Lu, T. Z.; Xie, X. M.; Zhang, Y. C.; Zhou, G. G.; Wu, K. Y.; Guo, J. R. Nanoscale liquid hydrocarbon adsorption on clay minerals: a molecular dynamics simulation of shale oils. *Chem. Eng. J.* **2021**, *420* (3), 127578.
(64) Ross, D. J.; Bustin, R. M. The importance of shale composition and pore structure upon gas storage potential of shale gas reservoirs. *Mar. Petrol. Geol.* **2009**, *26* (6), 916−927.
(65) Rani, S.; Padmanabhan, E.; Prusty, B. K. Review of gas adsorption in shales for enhanced methane recovery and CO_2 storage. *J. Petrol. Sci. Eng.* **2019**, *175*, 634−643.
(66) Chen, F. R.; Jiang, C. F.; Shi, P.; Chen, J. F.; Dong, J.; Feng, D. J.; Cheng, H. Y. Geochemical characteristics of terrestrial shale gas and its production prediction significance in the Ordos Basin. *China. J. Nat. Gas Geosci.* **2016**, *1* (6), 425−433.
(67) (in Chinese with English abstract) Meng, Q.; Wang, X. F.; Wang, X. Z.; Lei, Y. H.; Liu, P.; Zhang, L. X.; Jiang, C. F.; Gao, C. Biodegradation of light hydrocarbon (C5-C8) in shale gases from the Triassic Yanchang Formation, Ordos basin. *China. J. Nat. Gas Sci.* **2018**, *51*, 183−194.
(68) Rexer, T. F. T.; Benham, M. J.; Aplin, A. C.; Thomas, K. M. Methane adsorption on shale under simulated geological temperature and pressure conditions. *Energy Fuel.* **2013**, *27*, 3099−3109.
(69) (in Chinese with English abstract) Dai, J. X.; Qi, H. F. The δ^{13}C-Ro relation of coal-formed hydrocarbon in China. *China Sci. Bull.* **1989**, *34* (9), 110−113.
(70) Yang, R.; He, S.; Hu, Q. H.; Hu, D. F.; Yi, J. Z. Geochemical characteristics and origin of natural gas from Wufeng-Longmaxi shales of the Fuling gas field, Sichuan Basin (China). *Int. J. Coal Geol.* **2017**, *171*, 1−11.
(71) (in Chinese with English abstract) Li, W.; Lu, S.; Li, J.; Zhang, P.; Wang, S.; Feng, W.; Wei, Y. Carbon isotope fractionation during shale gas transport: Mechanism, characterization and significance. *China Earth Sci.* **2020**, *63*, 674−689.
(72) Li, W. B.; Lu, S. F.; Li, J. Q.; Wei, Y. B.; Feng, W. J.; Zhang, P. F.; Song, Z. J. Geochemical modeling of carbon isotope fractionation during methane transport in tight sedimentary rocks. *Chem. Geol.* **2021**, *566*, No. 120033.
(73) Qin, S.; Tang, X.; Song, Y.; Wang, H. Distribution and fractionation mechanism of stable carbon isotope of coalbed methane. *Sci. China Ser. D-Earth Sci.* **2006**, *49*, 1252−1258.
(74) Gunter, B. D.; Gleason, J. D. Isotope fractionation during gas chromatographic separations. *J. Chromatogr. Sci.* **1971**, *3*, 191−192.
(75) (in Chinese with English abstract) Han, H.; Zhong, N.; Wang, Y.; Huang, C. Characteristics of Stable Carbon Isotope of Shale Gas and Their Application Prospects. *Geol. Sci. Technol. Inf.* **2014**, *33* (2), 134−139.
(76) Rahayudin, Y.; Kashiwaya, K.; Tada, Y.; Iskandar, I.; Koike, K.; Atmaja, R. W.; Herdianita, N. R. On the origin and evolution of geothermal fluids in the Patuha Geothermal Field, Indonesia based on geochemical and stable isotope data. *Appl. Geochem.* **2020**, *114*, No. 104530.
(77) Zou, Y. R.; Cai, Y.; Zhang, C.; Zhang, X.; Peng, P. Variations of natural gas carbon isotope-type curves and their interpretation - a case study. *Org. Geochem.* **2007**, *38*, 1398−1415.
(78) Cao, C. H.; Zhang, M. J.; Li, L. W.; Wang, Y. H.; Li, Z. P.; Du, L.; Holland, G.; Zhou, Z. Tracing the sources and evolution processes of shale gas by coupling stable (c, h) and noble gas isotopic compositions: cases from weiyuan and changning in sichuan basin, china. *J. Nat. Gas Sci. Eng.* **2020**, *78*, No. 103304.
(79) Whiticar, M. J. Carbon and hydrogen isotope systematics of bacterial formation and oxidation of methane. *Chem. Geol.* **1999**, *161*, 291−314.
(80) Rohrback, B. G.; Peters, K. E.; Kaplan, I. R. Geochemistry of artificially heated humic and sapropelic sediments II: oil and gas generation. *AAPG Bull.* **1984**, *68* (8), 961−970.
(81) Hill, R. J.; Tang, Y.; Kaplan, I. Insight into cracking based on laboratory experiments. *Org. Geochem.* **2003**, *34* (12), 1651−1672.
(82) Dai, J. X., Pei, X. Q., Qi, H. F. *China Natural Gas Geology*; Geology Press: Beijing, 1992; Vol. *1*, pp 65−87.
(83) (in Chinese with English abstract) Wei, X. F.; Guo, T. L.; Liu, R. B. Geochemical features of shale gas and their genesis in Jiaoshiba block of Fuling Shale Gasfield, Chongqing. *Nat. Gas Geosci.* **2016**, *27* (3), 539−548.
(84) (in Chinese with English abstract) Liu, Q. Y.; Jin, Z. J.; Li, H. L.; Wu, X. Q.; Tao, X. W.; Zhu, D. Y.; Meng, Q. Q. Geochemistry characteristics and genetic types of natural gas in central part of the Tarim Basin. *NW China. Mar. Petrol. Geol.* **2018**, *89* (1), 91−105.
(85) Zhang, K.; Jia, C.; Song, Y.; Jiang, S.; Jiang, Z.; Wen, M.; Liu, T. Analysis of Lower Cambrian shale gas composition, source and accumulation pattern in different tectonic backgrounds: a case study of Weiyuan Block in the Upper Yangtze region and Xiuwu Basin in the Lower Yangtze region. *Fuel* **2020**, *263*, No. 115978.
(86) Xia, X.; Chen, J.; Braun, R.; Tang, Y. Isotopic reversals with respect to maturity trends due to mixing of primary and secondary products in source rocks. *Chem. Geol.* **2013**, *339*, 205−212.
(87) Milkov, A. V.; Faiz, M.; Etiope, G. Geochemistry of shale gases from around the world: composition, origins, isotope reversals and rollovers, and implications for the exploration of shale plays. *Org. Geochem.* **2020**, *143*, No. 103997.

https://doi.org/10.1021/acsomega.3c08330
ACS Omega 2024, 9, 13764−13781